Article

CST–polymerase α-primase solves a second telomere end-replication problem

https://doi.org/10.1038/s41586-024-07137-1

Received: 26 July 2023

Accepted: 30 January 2024

Published online: 28 February 2024

Check for updates

Hiroyuki Takai[1,3], Valentina Aria[2,3], Pamela Borges[1], Joseph T. P. Yeeles[2]✉ & Titia de Lange[1]✉

Telomerase adds G-rich telomeric repeats to the 3′ ends of telomeres[1], counteracting telomere shortening caused by loss of telomeric 3′ overhangs during leading-strand DNA synthesis ('the end-replication problem'[2]). Here we report a second end-replication problem that originates from the incomplete duplication of the C-rich telomeric repeat strand (C-strand) by lagging-strand DNA synthesis. This problem is resolved by fill-in synthesis mediated by polymerase α-primase bound to Ctc1–Stn1–Ten1 (CST–Polα-primase). In vitro, priming for lagging-strand DNA replication does not occur on the 3′ overhang and lagging-strand synthesis stops in a zone of approximately 150 nucleotides (nt) more than 26 nt from the end of the template. Consistent with the in vitro data, lagging-end telomeres of cells lacking CST–Polα-primase lost 50–60 nt of telomeric CCCTAA repeats per population doubling. The C-strands of leading-end telomeres shortened by around 100 nt per population doubling, reflecting the generation of 3′ overhangs through resection. The measured overall C-strand shortening in the absence of CST–Polα-primase fill-in is consistent with the combined effects of incomplete lagging-strand synthesis and 5′ resection at the leading ends. We conclude that canonical DNA replication creates two telomere end-replication problems that require telomerase to maintain the G-rich strand and CST–Polα-primase to maintain the C-strand.

Human telomeres are composed of long arrays of duplex TTAGGG repeats ending in a 3′ overhang of the G-rich strand (Fig. 1a). The 3′ overhangs enable telomeres to adopt the protective t-loop configuration[3,4] and serve as primers for telomerase. During the replication of telomeres, the C-rich 5′-ended strand is the template for leading-strand DNA synthesis, whereas the TTAGGG repeat strand templates lagging-strand DNA synthesis (Fig. 1a). The end-replication problem was originally proposed to involve removal of the RNA primer of the most terminal Okazaki fragment, predicting cumulative sequence loss at the 5′ ends of lagging-strand products[5,6] (Extended Data Fig. 1a). Telomerase was initially proposed to solve this problem by elongating the G-rich strand before DNA replication[7], thereby extending the template for Okazaki fragment synthesis (Extended Data Fig. 1b). However, once it had become clear that telomeres of most organisms carry constitutive 3′ overhangs, which cannot be regenerated by leading-strand DNA synthesis, a new version of the end-replication problem emerged[2] (Fig. 1a and Extended Data Fig. 1c). In this version, the sequence loss—equivalent to the length of the 3′ overhang—occurs on the leading strand and is counteracted by telomerase adding a 3′ overhang to the leading-strand product[2] (Fig. 1a). In agreement, human telomerase was shown to act after DNA replication, extending the 3′ ends of both leading-strand and lagging-strand DNA synthesis products[8,9]. Initial 5′ end resection of the leading-strand products, presumed to be blunt, is needed for their extension by telomerase and serves to regenerate the 3′ overhangs in cells lacking telomerase[10–13] (Fig. 1a). According to this scenario, telomerase solves the leading-strand end-replication problem[2,13] and the constitutive 3′ overhangs solve the lagging-strand problem (Fig. 1a). In agreement with the idea that lagging-strand synthesis can initiate on the 3′ overhang, RNA primers have been observed along the 3′ overhangs of human telomeres[14] (Fig. 1a and Extended Data Fig. 1). However, whether these priming events resulted from canonical lagging-strand DNA replication has not been established. Here we argue that the measured priming events reflected CST–Polα-primase fill-in synthesis. We use an in vitro DNA replication system to determine priming sites for the last Okazaki fragments generated by the replisome and identify an additional end-replication problem that it is solved by CST–Polα-primase in vivo.

To determine how the replisome behaves at the end of a linear DNA template, we used an in vitro reconstituted DNA replication system to map the ends of nascent lagging and leading strands. In this system, replisomes are assembled with purified *Saccharomyces cerevisiae* proteins that perform complete leading-strand and lagging-strand replication at the in vivo rate[15,16]. Origin-dependent DNA replication was performed on linear templates that carried either a 100-nt 3′ overhang or the same DNA sequence in duplex form (no overhang) (Fig. 1b,c and Extended Data Fig. 2a). Prior to analysis using denaturing polyacrylamide gels, the radiolabelled replication products were nicked with Nb.BbvCI or Nt.BbvCI, which liberate nascent lagging- and leading-strand ends, respectively (Fig. 1b,c). Reaction products digested with Nt.BbvCI were insensitive to RNase HII and migrated as single bands of close to the expected lengths for fully-extended replication products (236 and 336 nt for templates with and without overhang,

[1]Laboratory for Cell Biology and Genetics, Rockefeller University, New York, NY, USA. [2]Medical Research Council Laboratory of Molecular Biology, Cambridge, UK. [3]These authors contributed equally: Hiroyuki Takai, Valentina Aria. ✉e-mail: jyeeles@mrc-lmb.cam.ac.uk; delange@rockefeller.edu

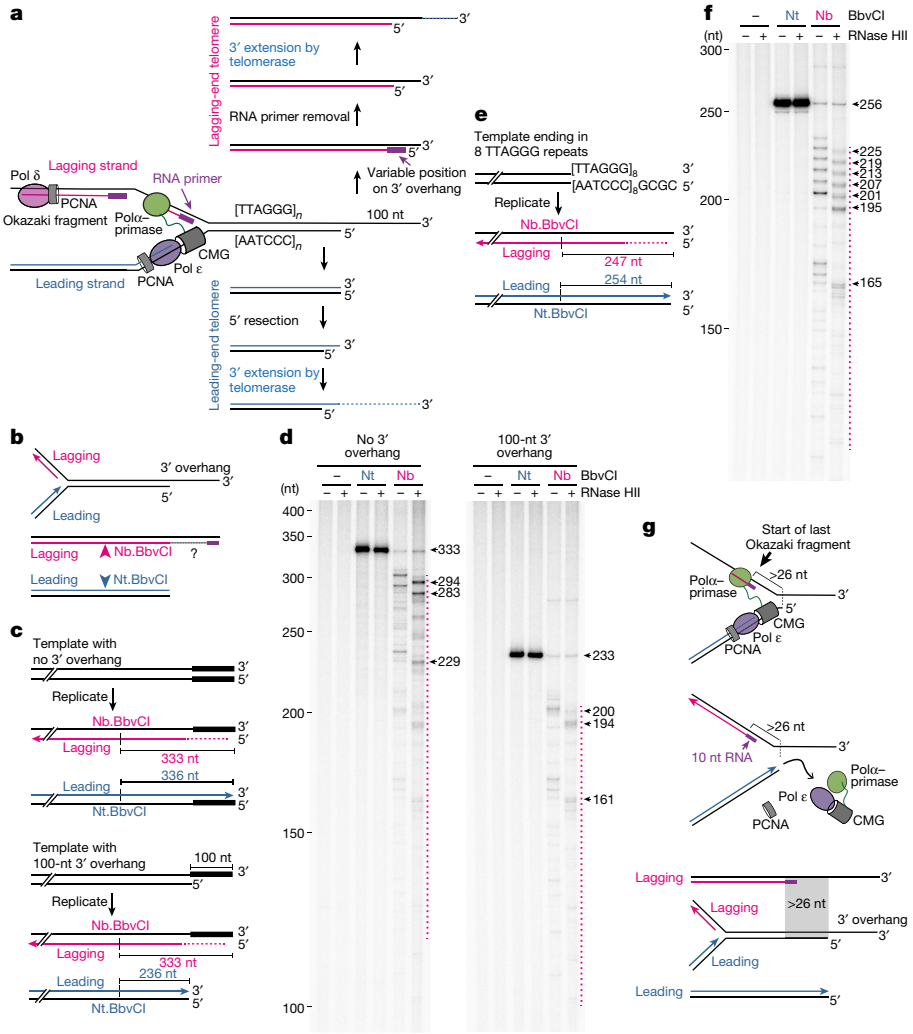

Fig. 1 | In vitro replication of linear templates reveals a second end-replication problem. a, Schematic of the end-replication problem at a telomere with a 100-nt 3′ overhang and its solution by telomerase prior to this study (modified from ref. 2). **b**, Schematic of the in vitro replication approach to determine the products formed by the replisome at DNA ends. **c**, Diagrams of replication templates and anticipated leading and lagging-strand products. The location of the BbvCI site and the anticipated products of nicking by Nb.BbvCI and Nt.BbvCI are shown. **d**, Denaturing 5.5% polyacrylamide–urea gel analysis of a 30-min replication reaction performed on the templates illustrated in **c**. Products were post-replicatively digested with Nt.BbvCI (Nt) or Nb.BbvCI (Nb) and RNase HII as indicated. The length in nucleotides of major reaction products, derived from the plots in Extended Data Fig. 2b, are shown. The distribution of Nb.BbvCI-dependent products is marked by a dashed line. **e**, Diagram of a replication template containing eight terminal TTAGGG repeats and anticipated leading and lagging-strand products after digestion with Nb.BbvCI and Nt.BbvCI. **f**, Denaturing 5.2% polyacrylamide–urea gel analysis of a replication reaction performed on the template illustrated in **e**, analysed as in **d**. **g**, Schematic illustrating that the last Okazaki fragment (after primer removal) starts more than 26 nt from the 5′ end of the template and the terminal structures predicted to be created by replication of a linear DNA. To enable clear visualization of the Nb.BbvCI products, the Nt.BbvCI product bands are saturated in **d** and **f**.

respectively) (Fig. 1d), establishing that leading-strand DNA synthesis efficiently completes the replication of linear DNA templates, as predicted by data on yeast telomere replication[17,18]. By contrast, digestion of replication products with Nb.BbvCI generated ladders of bands that varied in intensity and were sensitive to RNase HII treatment, confirming that they corresponded to the 5′ ends of nascent lagging strands. The shortest RNase HII-sensitive products were 150–200 nucleotides shorter than the maximum theoretical Nb.BbvCI cleavage product (Fig. 1d and Extended Data Fig. 2b). Notably, after RNase HII digestion, the longest RNase HII-sensitive products were around 30 nt shorter than the corresponding leading-strand products, regardless of the presence of a 3′ overhang (Fig. 1d and Extended Data Fig. 2b). These results reveal that the core eukaryotic replisome initiates the final Okazaki fragment at multiple positions within 150–200 nucleotides of the end of a linear template. Additionally, they show that the replisome is unable to initiate new Okazaki fragments once it gets to within around 20 nt of the end of the leading-strand template and consequently it cannot sustain canonical lagging-strand synthesis along a 3′ overhang.

To mimic the replication of telomere ends, we generated a linear template with eight TTAGGG repeats at the 3′ end of the lagging-strand template (Fig. 1e). Replication of this template produced six evenly spaced RNase HII-sensitive products (Fig. 1f and Extended Data Fig. 2c). The lengths of these products indicate that they represent Okazaki fragments initiated within the telomeric repeats, probably using ATP to begin primer synthesis (Extended Data Fig. 2d). Notably, the presence of 6, rather than 8, bands suggests that the replisome is unable to utilize the final 16 nt of TTAGGG repeat DNA to initiate new Okazaki fragments (Extended Data Fig. 2d), even when the concentration of Polα-primase in the reaction was increased fourfold (Extended Data Fig. 2e,f). To further validate this conclusion, we generated a template with an identical sequence but with 121 bp of double stranded DNA downstream of the 8 TTAGGG repeats and observed 8 evenly spaced RNase HII-sensitive

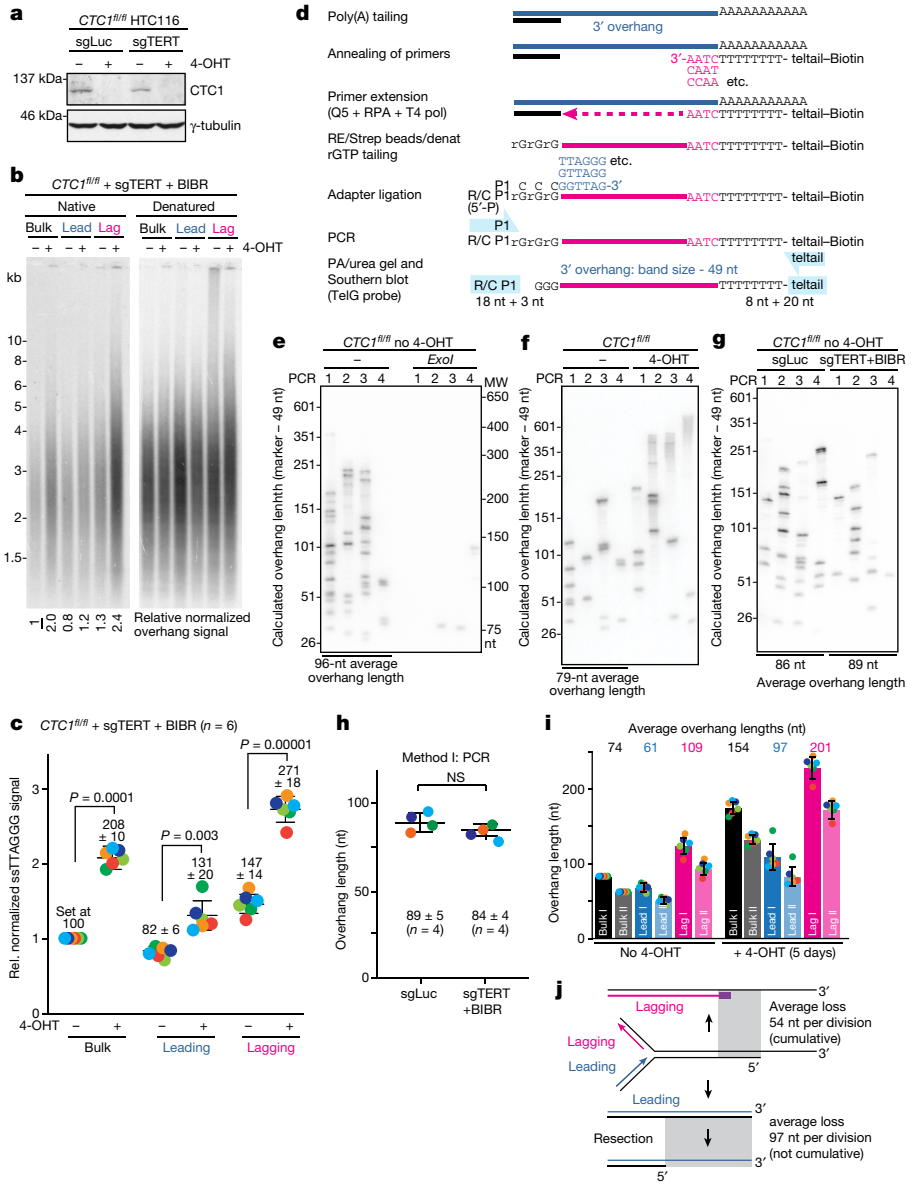

Fig. 2 | C-strand loss at leading-end and lagging-end telomeres in absence of CST. a, CTC1 immunoblot in *CTC1*$^{fl/fl}$ HCT116 cells with bulk CRISPR–Cas9 knockout of *TERT* (sgTERT). sgLuc, control sgRNA targeting the luciferase gene. 4-OHT induces Cre expression. **b**, In-gel overhang assay for relative overhang signals of CsCl-gradient-fractionated leading-end (lead) and lagging-end (lag) telomeres of the indicated cells. Left, TelC hybridization to detect the G-strand overhang. Right, gel probed with TelC after in situ denaturation, to detect total telomeric DNA for normalization (normalized values relative to lane 1). Cells were at population doubling 5 after *CTC1* deletion. **c**, Relative overhang signals from six biological replicates as in **b**. Data are mean ± s.d. *P* values determined by unpaired two-sided *t*-test. **d**, PCR assay for telomeric 3′ overhang length (method I). **e**, PCR overhang assays (four PCRs per sample) on genomic DNA with and without pre-treatment with *E. coli* ExoI showing the specificity for 3′ overhangs. Right, molecular mass marker. Left, calculated 3′ overhang length. Bottom, average 3′ overhang length. **f**, PCR overhang assay detects elongated 3′ telomeric overhang upon *CTC1* deletion as in **e**. The assay sensitivity for long overhangs is unknown. **g**, PCR overhang assay on DNA from *CTC1*$^{fl/fl}$ cells (no 4-OHT) with and without telomerase activity as in **e**. **h**, Mean 3′ overhang lengths from 4 biological replicates (4 PCRs per replicate) as in **g**. NS, not significant based on unpaired two-sided *t*-test. Data are mean ± s.d. **i**, Absolute overhang lengths at leading-end and lagging-end telomeres in telomerase-deficient cells with and without CTC1. Relative values in **c** were calibrated using values for bulk telomeres in telomerase-deficient cells determined by method I in **i** (bulk I) and method II in Extended Data Fig. 6f (bulk II). Data are mean ± s.d. *P* values in **c**. **j**, Predicted C-strand sequence loss in telomerase-negative cells lacking CTC1 based on **i** and calculations in Extended Data Fig. 7.

products, demonstrating that Okazaki fragment synthesis was initiated on each of the 8 repeats (Extended Data Fig. 3a–c). Collectively, these data demonstrate that for terminal TTAGGG repeats, it is the proximity to the end of the template that renders them incompatible with Okazaki fragment initiation. This behaviour is consistent with recent cryo-electron microscopy structures of yeast and human replisomes containing Polα-primase[19]. In both structures, the primase active site is positioned approximately 75 Å from the point of template unwinding (Extended Data Fig. 3d). Consequently, in this configuration, it is unlikely that Polα-primase can prime within the last 20 nt of a linear template because the parental DNA duplex will be fully unwound before the template has reached the primase active site. Moreover, because the positioning of Polα-primase in the replisome is highly conserved between budding yeast and human (Extended Data Fig. 3d), it is reasonable to expect that during lagging-strand replication of telomeres, human replisomes will behave the same as budding yeast replisomes. Owing to this additional end-replication problem, the C-rich telomeric strand is predicted to continuously shorten by more than 26 nt, and

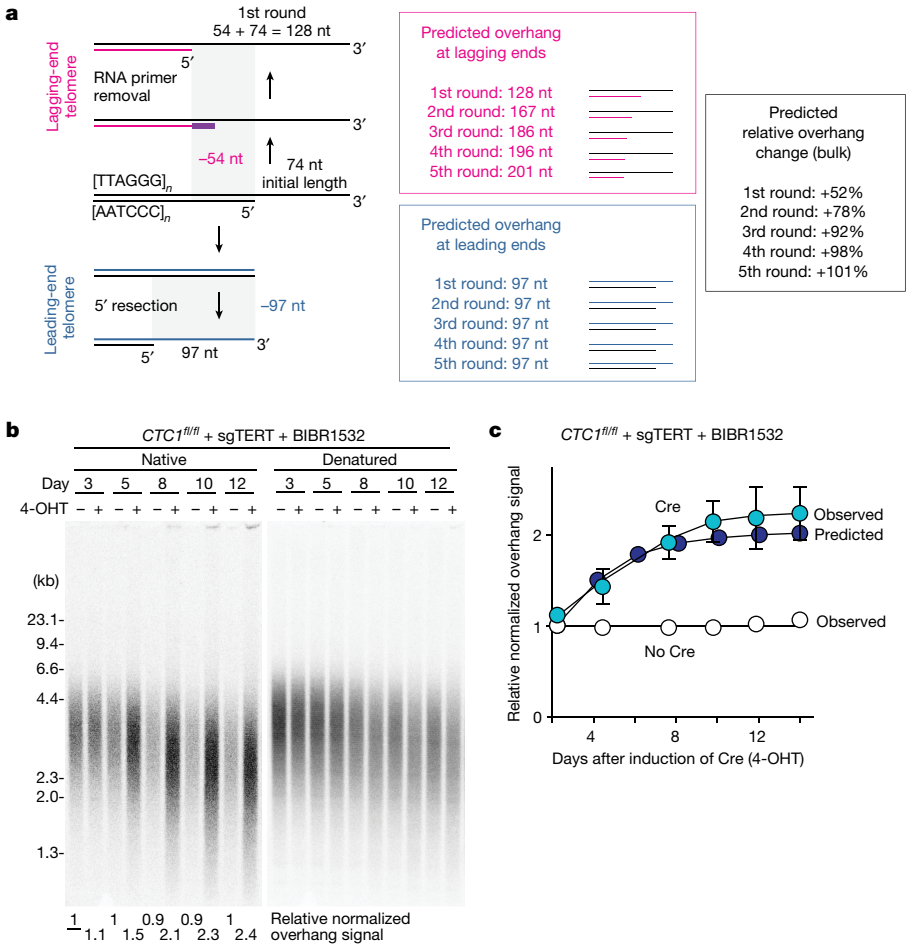

Fig. 3 | Telomeric overhangs elongate at the predicted rate after *CTC1* deletion. a, Predicted C-strand loss at leading-end and lagging-end telomeres in telomerase- and CTC1-deficient cells undergoing five cell divisions. The predicted relative overhang change (black) was calculated based on the initial overhang length (74 nt; Fig. 2i) and changes of the predicted overhang at lagging and leading ends (Fig. 2i,j and Extended Data Fig. 7). **b**, In-gel overhang assays on telomerase-deficient (sgTERT + BIBR1532 treatment) $CTC1^{fl/fl}$ cells (with or without 4-OHT treatment). Relative normalized overhang signals are shown below the gel with the first lane set to 1. **c**, Close agreement with the predicted (as in **a**, black) and observed 3′ overhang changes. Values are from three independent experiments as in **b**. Data are mean ± s.d.

this shortening will not be mitigated by extension of the G-rich strand by telomerase (Fig. 1g).

Sequence loss from the 5′ end of the C-rich telomeric strand can be counteracted by Polα-primase in association with the CST (Ctc1, Stn1 and Ten1) complex[20,21]. CST is a replication protein A (RPA)-like single stranded DNA-binding protein that interacts with Polα-primase and stimulates its activity[22–31]. At mammalian telomeres, CST–Polα-primase can fill in telomere ends that have been hyper-resected, thereby preventing excessive telomere shortening[10,11,32,33]. Prior work has shown that the C-rich strand progressively shortens when CST–Polα-primase fill-in is disabled[32,33] but the rate of shortening at leading-end and lagging-end telomeres and the cause of shortening remained unknown.

We set out to determine whether lagging-strand DNA synthesis results in shortened C-strands in vivo. CsCl gradients can be used to separate telomeres generated by leading-strand and lagging-strand DNA synthesis on the basis of their differential incorporation of BrdU[14] (Extended Data Fig. 4a). This method yields limited amounts of DNA, necessitating quantification of the 3′ overhangs by the sensitive in-gel hybridization method[10,34]. We applied this approach to $CTC1^{fl/fl}$ HCT116 colon carcinoma cells[32] from which *CTC1* can be deleted upon induction of Cre with tamoxifen (4-OHT). $CTC1^{fl/fl}$ cells express telomerase but were rendered telomerase-negative through bulk CRISPR–Cas9 knockout of TERT and further inhibition of telomerase activity with BIBR1532[35] so that no extension of the 3′ overhangs by telomerase can take place (Fig. 2a and Extended Data Fig. 4b,c). The relative 3′ overhang signals from six independent experiments showed that deletion of *CTC1* induced a substantial increase in the relative 3′ overhang signals at both leading-end and lagging-end telomeres, as expected from previous studies[10,11,32,33] (Fig. 2b,c).

Because the in-gel detection of telomeric overhangs yields only relative values, we aimed to determine the absolute length of the 3′ overhang in at least one of the samples to calibrate the relative overhang values from the in-gel assays. We developed two methods to measure absolute lengths of the 3′ overhang in cells containing CST in the presence or absence of telomerase activity. The first method, inspired by primer extension experiments performed with yeast and human telomeric DNA[34,36], is based on a PCR amplification of a fill-in product generated with poly(A) tailed 3′ overhangs as a template (Fig. 2d). This method relies on annealing the poly(A)-tailed telomeres to a set of oligodT primers that represent the six possible 3′ end sequences of telomeres followed by primer extension by bacterial DNA polymerases that lack strand-displacement activity. The oligodT primers also contained a specific sequence for PCR (teltail) and a 5′ biotin for isolation of the extension products. The extension products are tailed with GTP ribonucleotide (rGTP) and ligated to an adapter, enabling generation of PCR products that can be analysed by probing blots of polyacrylamide–urea gels with a radiolabelled G-strand oligonucleotide. The method was tested on a telomere model substrate featuring a stretch of duplex

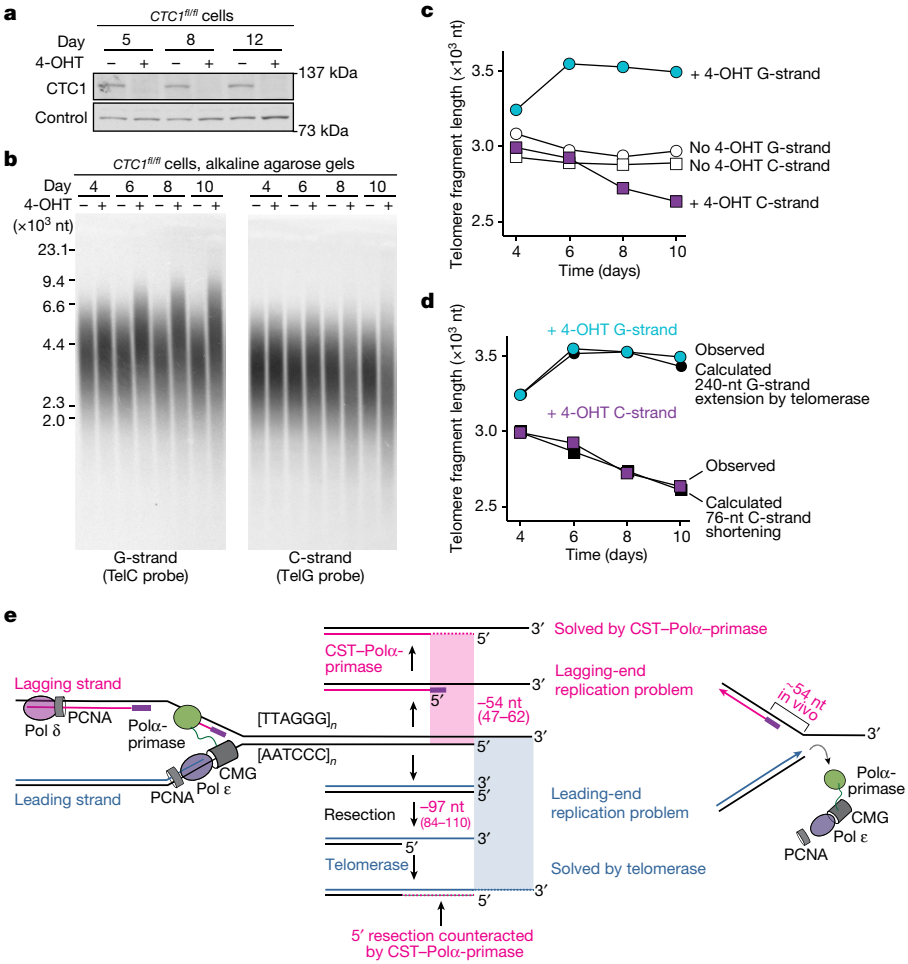

Fig. 4 | C-strand shortening at the predicted rate in absence of CST. **a**, Immunoblot for CTC1 in *CTC1*$^{fl/fl}$ HCT116 cells with and without induction of Cre with 4-OHT. A non-specific band was used as a loading control. **b**, Alkaline agarose gel analysis of the G- and C-rich telomeric restriction fragments in telomerase-positive *CTC1*$^{fl/fl}$ cells with or without 4-OHT treatment. Left, gel hybridized with TelC to detect the G-strands. Right, duplicate gel probed with TelG to detect the C-strands. **c**, Graph showing the changes in the lengths of the G- and C-strands as determined in **b**. **d**, Close agreement of the observed length changes in CTC1-deficient cells with calculated length changes based on C-strand shortening of 76 nt per population doubling and G-strand elongation of 240 nt per population doubling by telomerase (see Extended Data Fig. 9). **e**, Schematic illustrating the two end-replication problems. The leading-end replication problem is solved by telomerase elongating the G-rich strand. CST–Polα-primase provides the solution to the lagging-strand replication problem that results from the position of the last Okazaki fragment synthesized by the replisome. In addition, CST–Polα-primase counteracts C-strand sequence loss resulting from 5′ end resection at the leading-end telomeres.

telomeric repeats and a $[TTAGGG]_n$ 3′ overhang of 56 nt (Extended Data Fig. 5a,b). This substrate yielded a PCR product of the expected length that was not observed when the 3′ overhang was first removed with the *Escherichia coli* 3′ exonuclease ExoI (Extended Data Fig. 5b).

DNA from CTC1-proficient cells yielded sets of PCR products that were largely absent when the DNA was first treated with ExoI to remove the 3′ overhangs (Fig. 2e). As is the case for the PCR products in the single telomere length analysis[37] (STELA) assay, parallel PCRs on the same DNA sample yielded different sets of bands, indicating that each band is likely to represent the 3′ overhang of a single telomere. As expected, the PCR products from cells lacking CTC1 were substantially longer (Fig. 2f). Control experiments with oligonucleotides designed to represent fill-in products from 3′ overhangs with 5–15 repeats indicated that the assay was robust, yielding products with the expected length and intensity (Extended Data Fig. 5c,d). An oligonucleotide containing 20 repeats was also readily detected, although with greater variation in intensity (Extended Data Fig. 5d), indicating that some of the products obtained from longer 3′ overhangs could escape detection. Using this approach, the average lengths of the 3′ overhangs in genomic DNAs from *CTC1*$^{fl/fl}$ and *CTC1*$^{fl/fl}$ cells treated with single guide RNA (sgRNA) targeting *TERT* (sgTERT) and BIBR1532 (but not with 4-OHT) were determined in four independent experiments (Fig. 2g,h). The average overhang length of each DNA sample was derived by summing the sizes of all bands observed in 4 PCRs, dividing the sum by the number of detected bands, and subtracting the 49-nt non-telomeric sequences in the products (Fig. 2d–g). The average 3′ overhang lengths in cells with and without telomerase were 89 and 84 nt, respectively (Fig. 2h). The similar sizes of the 3′ overhangs in cells with and without telomerase is consistent with data from in-gel hybridization experiments that showed a minimal difference in the relative 3′ overhang signals (Extended Data Fig. 5e).

In an orthogonal approach to determine the absolute 3′ overhang lengths, we measured the shortening of the G-rich telomeric strand upon removing the 3′ overhang by treating native DNA with ExoI. This method is reminiscent of experiments done on yeast telomeres, which are sufficiently short to be analysed by PCR before and after ExoI treatment[17]. To analyse the longer telomeres of HCT116 cells, we treated genomic DNA with ExoI, digested the product with MboI and AluI to generate telomeric restriction fragments, and measured the reduction in the size of the telomeric G-strand on alkaline agarose gels by in-gel hybridization (Extended Data Fig. 6). This method was tested on the

model telomere with a 3′ overhang of defined length (Extended Data Fig. 6a). ExoI digestion of the linear model telomere bearing a 3′ overhang reduced the size of the G-strand by 57 nt, which is close to the expected value of 56 nt (Extended Data Fig. 6a). We applied the ExoI method to DNA from CTC1-proficient cells with and without telomerase (Extended Data Fig. 6b–e), which showed 3′ overhang lengths of 79 and 64 nt for cells with and without telomerase, respectively (Extended Data Fig. 6f). These values are close to those obtained by the PCR method.

The overhang lengths in CTC1-proficient cells lacking telomerase activity determined by the two methods were used to calibrate the relative overhang signals measured on separated leading-end and lagging-end telomeres (Fig. 2i). According to this analysis, telomerase-negative cells lacking CTC1 have 3′ overhangs of approximately 97 and 201 nt at their leading-end and lagging-end telomeres, respectively (Fig. 2i). Taking these values into account, our modelling (Extended Data Fig. 7) indicates that the leading-end telomeres lose 97 nt of C-rich sequences due to resection, whereas the lagging-end telomeres lose around 54 nt (Fig. 2j). The finding of C-strand sequence loss at lagging-end telomeres of cells lacking CTC1 is consistent with the in vitro analysis of the lagging-end replication products. We cannot exclude that the loss of C-strand sequences from the lagging-end telomeres is due to exonucleolytic attack, rather than a deficiency in lagging-strand replication. However, we consider this possibility unlikely because it would require a regulatory mechanism that enforces distinct outcomes of resection at the leading-end and lagging-end telomeres. Furthermore, a previous study showed that no resection occurred at lagging-end telomeres in human cells[14], although lagging-end resection was observed in mouse cells[10]. This difference in resection at human and mouse telomeres may be explained on the basis of the recently identified ATC-5′-phosphate (ATC-5′-P)-binding site in POT1 proteins[38] (referred to as the POT-hole). End binding by the POT-hole could block 5′ resection of the last Okazaki fragment, which is predicted to end in ATC-5′-P[21]. Whereas human telomeres have only one POT1 protein that has the POT-hole, mouse telomeres have two POT1 proteins[39] one of which lacks a POT-hole[38], possibly leading to less repression of resection lagging-strand mouse telomeres.

On the basis of the inferred average C-strand shortening caused by resection at the leading ends (97 nt) and incomplete synthesis at the lagging ends (54 nt) (Fig. 2j), we predicted how the length of the 3′ overhang would change with cell divisions when CTC1 is absent from telomerase-negative cells (Fig. 3a and Extended Data Fig. 7). We then used the in-gel overhang assay to measure the relative normalized 3′ overhang signals in telomerase-negative cells from which *CTC1* was deleted (Fig. 3b). Results from three independent experiments showed that the observed relative 3′ overhang change was nearly identical to the predicted change (Fig. 3c).

To further test whether the shortening of telomeric DNA in vivo is consistent with the predictions in Fig. 2j, the length changes of G- and C-rich strands were examined after *CTC1* deletion from telomerase-positive cells (Fig. 4a,b and Extended Data Fig. 8a,b). The G-strand was rapidly extended by around 240 nt per population doubling when *CTC1* was deleted, consistent with the lack of inhibition of telomerase by CST[20,21] (Fig. 4a–c and Extended Data Figs. 8a–c and 9). As previously observed[32,33], the C-strand shortened, while the G-strand elongated, confirming that the replisome is incapable of initiating Okazaki fragment synthesis on the 3′ overhang. On the basis of the inferred rate of C-strand sequence loss at the lagging- and leading-end telomeres, the overall rate of C-strand shortening is predicted to be approximately 76 nt per population doubling, which is close to the observed rate of C-strand shortening (Fig. 4d and Extended Data Fig. 8c).

The data reported here indicate that DNA replication creates a dual problem at telomere ends (Fig. 4e). The results of in vitro replication verify the long-held view that leading-strand replication leads to loss of the G-rich 3′ overhang sequence at one daughter telomere, which represents the end-replication problem that can be solved by telomerase. We document a second end-replication problem in vitro and in vivo that results from the inability of lagging-strand DNA synthesis to synthesize a C-strand of the same length as the parental C-strand (Fig. 4e). Our data indicate that CST–Polα-primase counteracts this C-strand loss through fill-in synthesis at lagging-end telomeres. CST–Polα-primase-mediated fill-in also mitigates C-strand loss at the leading-end telomeres where resection generates the 3′ overhang used by telomerase[10,11,32,33] (Fig. 4e). Together, these processes shorten the telomeric C-strand by approximately 76 nt per population doubling in HCT116 cells. In keeping with the critical role of CST–Polα-primase in solving the second end-replication problem, defects in this pathway lead to telomere biology disorders—predominantly Coats plus syndrome[40] and, more rarely, dyskeratosis congenita (reviewed in ref. 21). It was proposed that CST–Polα-primase evolved in the last eukaryotic common ancester (or its Asgard archaeal ancestor) to maintain the 5′ ends of linear chromosomes[21,25]. Our data argue for this view, since the lagging-strand end-replication problem is likely to have threatened the maintenance of the first linear chromosomes.

Online content

Any methods, additional references, Nature Portfolio reporting summaries, source data, extended data, supplementary information, acknowledgements, peer review information; details of author contributions and competing interests; and statements of data and code availability are available at https://doi.org/10.1038/s41586-024-07137-1.

1. Greider, C. W. & Blackburn, E. H. Identification of a specific telomere terminal transferase activity in Tetrahymena extracts. *Cell* **43**, 405–413 (1985).
2. Lingner, J., Cooper, J. P. & Cech, T. R. Telomerase and DNA end replication: no longer a lagging strand problem. *Science* **269**, 1533–1534 (1995).
3. Griffith, J. D. et al. Mammalian telomeres end in a large duplex loop. *Cell* **97**, 503–514 (1999).
4. Doksani, Y., Wu, J. Y., de Lange, T. & Zhuang, X. Super-resolution fluorescence imaging of telomeres reveals TRF2-dependent T-loop formation. *Cell* **155**, 345–356 (2013).
5. Watson, J. D. Origin of concatemeric T7 DNA. *Nat. New Biol.* **239**, 197–201 (1972).
6. Olovnikov, A. M. A theory of marginotomy. The incomplete copying of template margin in enzymic synthesis of polynucleotides and biological significance of the phenomenon. *J. Theor. Biol.* **41**, 181–190 (1973).
7. Greider, C. W. & Blackburn, E. H. Telomeres, telomerase and cancer. *Sci. Am.* **274**, 92–97 (1996).
8. Zhao, Y. et al. Telomere extension occurs at most chromosome ends and is uncoupled from fill-in in human cancer cells. *Cell* **138**, 463–475 (2009).
9. Hirai, Y., Masutomi, K. & Ishikawa, F. Kinetics of DNA replication and telomerase reaction at a single-seeded telomere in human cells. *Genes Cells* **17**, 186–204 (2012).
10. Wu, P., Takai, H. & de Lange, T. Telomeric 3′ overhangs derive from resection by Exo1 and Apollo and fill-in by POT1b-associated CST. *Cell* **150**, 39–52 (2012).
11. Wang, F. et al. Human CST has independent functions during telomere duplex replication and C-strand fill-in. *Cell Rep.* **2**, 1096–1103 (2012).
12. Dai, X. et al. Molecular steps of G-overhang generation at human telomeres and its function in chromosome end protection. *EMBO J.* **29**, 2788–2801 (2010).
13. Stewart, J. A., Wang, Y., Ackerson, S. M. & Schuck, P. L. Emerging roles of CST in maintaining genome stability and human disease. *Front. Biosci.* **23**, 1564–1586 (2018).
14. Chow, T. T., Zhao, Y., Mak, S. S., Shay, J. W. & Wright, W. E. Early and late steps in telomere overhang processing in normal human cells: the position of the final RNA primer drives telomere shortening. *Genes Dev.* **26**, 1167–1178 (2012).
15. Yeeles, J. T., Deegan, T. D., Janska, A., Early, A. & Diffley, J. F. Regulated eukaryotic DNA replication origin firing with purified proteins. *Nature* **519**, 431–435 (2015).
16. Yeeles, J. T. P., Janska, A., Early, A. & Diffley, J. F. X. How the eukaryotic replisome achieves rapid and efficient DNA replication. *Mol. Cell* **65**, 105–116 (2017).
17. Soudet, J., Jolivet, P. & Teixeira, M. T. Elucidation of the DNA end-replication problem in *Saccharomyces cerevisiae*. *Mol. Cell* **53**, 954–964 (2014).
18. Aria, V. & Yeeles, J. T. P. Mechanism of bidirectional leading-strand synthesis establishment at eukaryotic DNA replication origins. *Mol. Cell* **73**, 199–211 (2019).
19. Jones, M. L., Aria, V., Baris, Y. & Yeeles, J. T. P. How Pol α-primase is targeted to replisomes to prime eukaryotic DNA replication. *Mol. Cell* **83**, 2911–2924.e16 (2023).
20. Lim, C. J. & Cech, T. R. Shaping human telomeres: from shelterin and CST complexes to telomeric chromatin organization. *Nat. Rev. Mol. Cell Biol.* **22**, 283–298 (2021).
21. Cai, S. W. & de Lange, T. CST–Polα/Primase: the second telomere maintenance machine. *Genes Dev.* **37**, 555–569 (2023).
22. Goulian, M., Heard, C. J. & Grimm, S. L. Purification and properties of an accessory protein for DNA polymerase alpha/primase. *J. Biol. Chem.* **265**, 13221–13230 (1990).
23. Goulian, M. & Heard, C. J. The mechanism of action of an accessory protein for DNA polymerase alpha/primase. *J. Biol. Chem.* **265**, 13231–13239 (1990).
24. Lim, C. J. et al. The structure of human CST reveals a decameric assembly bound to telomeric DNA. *Science* **368**, 1081–1085 (2020).

25. Lue, N. F. Evolving linear chromosomes and telomeres: a C-strand-centric view. *Trends Biochem. Sci* **43**, 314–326 (2018).
26. Gao, H., Cervantes, R. B., Mandell, E. K., Otero, J. H. & Lundblad, V. RPA-like proteins mediate yeast telomere function. *Nat. Struct. Mol. Biol.* **14**, 208–214 (2007).
27. Miyake, Y. et al. RPA-like mammalian Ctc1–Stn1–Ten1 complex binds to single-stranded DNA and protects telomeres independently of the Pot1 pathway. *Mol. Cell* **36**, 193–206 (2009).
28. Surovtseva, Y. V. et al. Conserved telomere maintenance component 1 interacts with STN1 and maintains chromosome ends in higher eukaryotes. *Mol. Cell* **36**, 207–218 (2009).
29. Cai, S. W. et al. Cryo-EM structure of the human CST–Polα/primase complex in a recruitment state. *Nat. Struct. Mol. Biol.* **29**, 813–819 (2022).
30. He, Q. et al. Structures of the human CST–Polα-primase complex bound to telomere templates. *Nature* **608**, 826–832 (2022).
31. Zaug, A. J., Goodrich, K. J., Song, J. J., Sullivan, A. E. & Cech, T. R. Reconstitution of a telomeric replicon organized by CST. *Nature* **608**, 819–825 (2022).
32. Feng, X., Hsu, S. J., Kasbek, C., Chaiken, M. & Price, C. M. CTC1-mediated C-strand fill-in is an essential step in telomere length maintenance. *Nucleic Acids Res.* **45**, 4281–4293 (2017).
33. Takai, H. et al. A POT1 mutation implicates defective telomere end fill-in and telomere truncations in Coats plus. *Genes Dev.* **30**, 812–826 (2016).
34. McElligott, R. & Wellinger, R. J. The terminal DNA structure of mammalian chromosomes. *EMBO J.* **16**, 3705–3714 (1997).
35. Damm, K. et al. A highly selective telomerase inhibitor limiting human cancer cell proliferation. *EMBO J.* **20**, 6958–6968 (2001).
36. Larrivée, M., LeBel, C. & Wellinger, R. J. The generation of proper constitutive G-tails on yeast telomeres is dependent on the MRX complex. *Genes Dev.* **18**, 1391–1396 (2004).
37. Baird, D. M., Rowson, J., Wynford-Thomas, D. & Kipling, D. Extensive allelic variation and ultrashort telomeres in senescent human cells. *Nat. Genet.* **33**, 203–207 (2003).
38. Tesmer, V. M., Brenner, K. A. & Nandakumar, J. Human POT1 protects the telomeric ds-ss DNA junction by capping the 5′ end of the chromosome. *Science* **381**, 771–778 (2023).
39. Hockemeyer, D., Daniels, J. P., Takai, H. & de Lange, T. Recent expansion of the telomeric complex in rodents: two distinct POT1 proteins protect mouse telomeres. *Cell* **126**, 63–77 (2006).
40. Anderson, B. H. et al. Mutations in CTC1, encoding conserved telomere maintenance component 1, cause Coats plus. *Nat. Genet.* **44**, 338–342 (2012).

Methods

Construction of replication templates

The 3′ overhang and no-overhang templates used for in vitro DNA replication reactions were constructed by ligating oligonucleotides to the plasmid vVA25 following its linearization with SapI. To generate vVA25, a single BbvCI site was inserted ~200 nt upstream of the SapI restriction site in vVA22[18]. For the 3′ overhang template, a 25 bp duplex with a 100-base 3′ overhang was generated by annealing oligonucleotide VA67 (Sigma) and 3′ overhang (IDT). To generate a blunt-ended template with the same sequence as the 3′ overhang, oligonucleotide 3′ overhang was annealed to oligonucleotide JY556 (IDT). Annealing was performed by heating the oligonucleotides to 85 °C for 5 min and then slow cooling to room temperature in 200 mM NaCl, 5 mM EDTA. Annealed oligonucleotides were then ligated onto SapI-linearized vVA25. For the 3′ overhang template, ligation (250 µl reaction) was performed overnight at 16 °C in 1× T4 Ligase buffer with 50 nM SapI-linearized vVA25, 1.25 µM annealed oligonucleotides and 12,000 units T4 Ligase (NEB). For the no-overhang template, ligation (200 µl reaction) was performed overnight at 16 °C in 1× T4 Ligase buffer supplemented with 5 mM magnesium acetate and 0.5 mM ATP, 62.5 nM SapI-linearized vVA25, 1.56 µM annealed oligonucleotides and 12,000 units T4 Ligase (NEB). Ligation reactions were quenched by addition of EDTA to 25 mM and proteins were digested by incubation at 37 °C for 20 min with 0.1% SDS and 20 units per ml proteinase K (NEB). Unligated oligonucleotides were removed by gel filtration through a 50 cm × 0.7 cm Sepharose 4B column (Sigma) equilibrated in 5 mM Tris-HCl (pH 8), 0.1 mM EDTA.

To construct in vitro DNA replication templates containing human telomeric repeats, 8 TTAGGG repeats flanked by an AscI restriction site were inserted into vVA25 ~250 bp downstream of the BbvCI site. The sequence of the resulting plasmid was verified by Sanger and Nanopore sequencing (Source Bioscience). Linear templates were prepared by digesting CsCl density gradient purified DNA with AscI (NEB) (terminal repeats template) or PciI (NEB) (internal repeats template). Digest were quenched by addition of EDTA to 25 mM and proteins were digested by incubation at 37 °C for 40 min following addition of SDS and proteinase K (NEB) to 0.25% and 20 units per ml respectively. Proteins were removed by phenol:chloroform:isoamyl alcohol (25:24:1) (PCI) (Sigma) extraction followed by ethanol precipitation. DNA was resuspended in 10 mM Tris-Cl (pH 8), 1 mM EDTA.

Oligonucleotides used for generation of DNA termini: VA67, 5′-TAGTCCATCGGTTTTGCCATAAGAC-3′; 3′ overhang, 5′-[Phos]GCTG TCTTATGGCAAAACCGATGGACTATGTTTCGGGTAGCACCAGGAGTCT GTAGCACGTGCATCTCAACGTGGCGTGAGTACCTTTTAATCACCGCTT CATGCTAAGGATCTGGCTGCATGCTATG-3′; JY556 5′-CATAGCATG CAGCCAGATCCTTAGCATGAAGCGGTGATTAAAAGGTACTCACGCCAC GTTGAGATGCACGTGCTACAGACTCCTGGTGCTACCCGAAACATAGTC CATCGGTTTTGCCATAAGAC-3′.

Standard replication reaction

Standard replication reactions were carried out as reported previously[18,41] with minor alterations. MCM loading and phosphorylation was performed in a reaction (55 µl) containing: 25 mM Hepes-KOH, pH 7.6; 100 mM potassium glutamate; 40 mM KCl; 0.01% NP-40-S; 1 mM DTT; 10 mM magnesium acetate; 0.1 mg ml^{-1} BSA; 3 mM ATP; 3 nM DNA template; 75 nM Cdt1-Mcm2-7; 40 nM Cdc6; 20 nM ORC; 25 mM DDK. After incubation at 24 °C for 10 min, S-CDK was added to 80 nM and the reaction was incubated for a further 5 min at 24 °C. The MCM loading reaction was then diluted fourfold into replication buffer to give final replication reaction conditions of: 25 mM Hepes-KOH, pH 7.6; 257 mM potassium glutamate; 10 mM KCl; 0.01% NP-40-S; 1 mM DTT; 10 mM magnesium acetate; 0.1 mg ml^{-1} BSA; 3 mM ATP; 0.2 mM GTP; 0.2 mM CTP; 0.2 mM UTP; 30 µM dATP; 30 µM dTTP; 30 µM dCTP; 30 µM dGTP; 0.75 nM DNA template; 18.75 nM Cdt1-Mcm2-7, 10 nM Cdc6; 5 nM ORC; 6.25 nM DDK; 20 nM S-CDK and either 33 nM α-[^{32}P]-dCTP (Hartmann Analytic SCP-205) (Fig. 1d) or 33 nM α-[^{32}P]-dATP (Hartmann Analytic SCP-203) (Fig. 1f and Extended Data Figs. 2e and 3b). Reactions (100 µl) were equilibrated at 30 °C and DNA replication was initiated by addition of replication proteins from a master mix to final concentrations of: 30 nM Dpb11; 100 nM GINS; 30 nM Cdc45; 10 nM Mcm10; 15 nM Pol ε; 20 nM Ctf4; 100 nM RPA; 20 nM RFC; 20 nM Tof1-Csm3; 20 nM PCNA; 5 nM Pol δ; 12.5 nM Sld3-7; 20 nM Sld2; 10 nM Mrc1; 20 nM Fen1; 20 nM Ligase and, unless indicated otherwise, 20 nM Polα-primase. Protein storage buffers additionally contributed approximately 12 mM NaCl/KCl and 25 mM potassium acetate/potassium glutamate to the reactions. Reactions were incubated at 30 °C for 30 min and were quenched by addition of EDTA to 50 mM. Proteins were removed by treatment with proteinase K (20 units per ml) (NEB) and SDS (0.25%) for 20 min at 37 °C followed by PCI extraction. Unincorporated nucleotide was removed using Illustra G-50 columns (GE Healthcare).

To map the 5′ and 3′ ends generated by the rightward moving replication fork when it runs off the end of the template, products were first digested (or mock digested) with RNase HII. Deproteinized reactions (63 µl) were incubated for 45 min at 37 °C in 1× ThermoPol buffer (NEB) with 15 units *E. coli* RNase HII (NEB M0288). Reactions were quenched by addition of EDTA to 50 mM and proteins were removed by treatment with proteinase K (20 units per ml) (NEB) and SDS (0.25%) for 10 min at 37 °C followed by PCI (Sigma) extraction. The DNA was ethanol precipitated following addition of 40 µg glycogen (Invitrogen) and was resuspended in 65 µl 1× rCutSmart buffer (NEB). Samples were divided into three 20 µl aliquots that were treated (or mock-treated) for 30 min at 37 °C with 10 units of Nt.BbvCI or Nb.BbvCI as indicated in the figures. Reactions were quenched by addition of EDTA to 50 mM and proteins were removed by treatment with proteinase K (20 units per ml) (NEB) and SDS (0.25%) for 10 min at 37 °C followed by PCI extraction and ethanol precipitation. For analysis through denaturing urea polyacrylamide gels, DNA was resuspended in 4 µl 10 mM Tris-Cl (pH 8), 1 mM EDTA and then supplemented with an equal volume of 2× loading buffer (95% formamide, 20 mM EDTA, 0.04% xylene cyanol, 0.04% bromophenol blue). After incubation at 95 °C for 5 min, products were immediately resolved on 5–5.5%, 40 cm×20 cm polyacrylamide (Bis-acrylamide 19:1, Fisher Scientific), 7 M Urea gels, run in 1× Tris-Borate-EDTA buffer (TBE) for 130 min at 40 W. Gels were dried under vacuum at 75 °C onto 3MM paper (Whatman) and imaged using Typhoon phosphorimager (GE Healthcare).

Analysis of in vitro DNA replication reactions

To generate normalized plots of DNA replication reactions, lane profiles were generated in ImageJ v_1.53a for each reaction condition and the molecular weight markers (50 bp ladder, NEB, N3236). Background was subtracted from each lane profile by subtracting the signal from the equivalent reaction condition (with or without RNase HII) but without BbvCI digestion using Excel. Following background subtraction, data were normalized by dividing the pixel intensity at each migration position by the pixel intensity of the most intense product band within the region displayed in each plot. To determine the approximate length of replication products in nucleotides, the relative migration distance (in centimetres) of each marker band was plotted against the $\log_{10}$ of its length (in nucleotides). Data were fit to a third order polynomial using Prism (GraphPad) and the resulting fits were used to interpolate product length values (in nucleotides) for every migration position of a given lane profile.

Cell culture, deletion of CTC1, depletion of telomerase and immunoblots

CTC1$^{fl/fl}$ HCT116 cells were generated by and obtained from Carolyn Price[32]. They are mycoplasma free and were cultured as described[32]. The cell line was confirmed based on Cre-deletion of *CTC1*. For *CTC1* deletion, the cells were treated with 0.5 µM 4-hydroxytamoxifen

(4-OHT) for 5 h to induce Cre recombinase. *CTC1* loss was verified by immunoblotting as described[33] using rabbit polyclonal antibody raised against recombinant full length human CTC1 (a gift from J. C. Zinder) at 1:3,000 dilution. The antibody for γ-tubulin (GTU-88; Sigma) was used at 1:10,000. *CTC1*$^{fl/fl}$ cells were rendered telomerase-deficient by bulk targeting of hTERT with lentiCRISPR v2 vector expressing Cas9 and sgRNAs (5′-ACACGGTGACCGACGCACTG-3′ and 5′-CTTGGTCTC GGCGTACACCG-3′). Telomerase was further inhibited using 16 μM BIBR1532[35] (TOCRIS 2981) in the media. TRAP assays for telomerase activity were performed using the TRAPeze kit (Millipore, S7700) according to the manufacture's instruction.

Overhang analysis of leading- and lagging-end telomeres

Isolation of genomic DNA and separation of leading-end and lagging-end telomeres were performed as described[10,14]. In brief, cells were cultured with 100 μM BrdU for 18 h, harvested, and genomic DNA was extracted. DNAs were digested with MboI and AluI and fractionated on CsCl density gradients and fractions were collected from the bottom of the centrifuge tubes. Telomeric DNA in each fraction was quantified by slot blot hybridization using γ-^{32}P-ATP end-labelled $[TTAGGG]_4$ (TelG probe) as described[10]. Leading-strand and lagging-strand peak fractions were pooled, dialysed to remove most CsCl, and DNAs were isolated by ethanol precipitation followed by suspension in TE. The pooled fractions were analysed using the in-gel overhang assay with a γ-^{32}P-ATP end-labelled $[AACCCT]_4$ (TelC probe) as described[10].

PCR assay for telomeric overhang (method I)

2×10^6 cells were trypsinized, pelleted, frozen in liquid N_2, and stored at −80 °C. For DNA extraction, the cell pellet was resuspended to 1 ml TLE buffer containing 10 mM Tris-HCl pH 7.8, 100 mM LiCl, 10 mM EDTA, and 100 μg ml^{-1} RNase A (Sigma, R5000). 1 ml TLES buffer (TLE + 0.1% (w/v) SDS) with 100 μg ml^{-1} proteinase K (Roche, 03115879001) was added and the suspension was incubated at 37 °C for 10 min. Genomic DNA was extracted with 2 ml PCI (Thermo Fisher, BP1752I), followed by DNA precipitation with 1/20 volume of 8 M LiCl and 1 volume of isopropanol. Genomic DNA was resuspended in 50 μl TE buffer containing 50 mM LiCl (50 mM LiCl-TE), 100 μg ml^{-1} RNase A, and 0.2 U μl^{-1} RNase H (NEB, M0297) and immediately used for the overhang assay as follows. Genomic DNA (30 μl) was poly(A) tailed using 20 units terminal transferase (TdT, NEB, M0315) and 0.2 mM dATP for 15 min at 37 °C in TdT buffer (20 mM Tris-HCl pH 7.9, 50 mM LiCl, 10 mM $MgCl_2$), followed by PCI extraction and isopropanol precipitation as above. DNA was resuspended in 40 μl Extension buffer (10 mM Tris-HCl pH 7.9, 50 mM LiCl, 10 mM $MgCl_2$, and 50 μg ml^{-1} BSA). The tailed DNA was annealed to 0.2 nM 5′ biotinylated teltail ss-adaptor at 21 °C for 10 min. Primer extension was performed with 0.006 U μl^{-1} Q5 (NEB, M0491) and 200 μM each of dATP/dCTP/dTTP at 21 °C for 10 min and an additional 15 min incubation with 25 nM recombinant human RPA (a gift from S. W. Cai) and 0.03 U μl^{-1} T4 DNA polymerase (NEB, M0203) at 37 °C. The teltail ss-adaptor (see below) is a mixture of single strand DNA oligonucleotides of 5′ biotinylated teltail[37] followed by $[T]_8$ and 4 nt of C-strand sequence in 6 permutations. Extended DNA was digested with AluI at 37 °C for 20 min to diminish the viscosity. Excess teltail ss-adaptor and short bulk genomic DNA fragments were removed by DNA size selection using 25 μl SPRI select (Beckman, 0.5× v/v SPRI beads to DNA suspension). After 2 washes with 80% ethanol according to the manufacturer's instructions, DNA was eluted in 60 μl 50 mM LiCl-TE buffer and the concentration of DNA was measured using NanoDrop (Thermo Fisher). A 0.5 μg sample of DNA was used for the subsequent steps. After capture of the products on washed Streptavidin beads (10 μl, Dynabeads M-280; Thermo Fisher, 11205D), the DNA was denatured with 150 mM NaOH for 5 min at 21 °C 2 times, neutralized with 2 washes with 1 M LiCl-TE buffer, one wash with 50 mM LiCl-TE, and resuspended in 50 μl TdT buffer containing 2 mM rGTP (Promega, E603B) and 20 U TdT at 37 °C for 15 min for rGTP tailing[42]. DNA-bound beads were rinsed 3 times with 50 mM LiCl-TE and ligated to P1 ds-adaptor for >1 h at 21 °C in Ligation mix (Extension buffer containing 20 nM P1 ds-adaptor, 200 μM ATP, 25% PEG 8000, 8 U μl^{-1} Salt-T4 DNA ligase (NEB M0467)). P1 ds-adaptors are double-strand (ds) splint adaptors that contain 5′ overhangs with the 6 permutations of the telomeric sequence (see below). 6 permutated upper oligonucleotides and the 5′ phosphorylated bottom-strand oligonucleotide were mixed, annealed, and kept as aliquots at −20 °C to avoid multiple freeze-thaw cycles. After 2 washes with 1 M LiCl-TE buffer, DNA-bound beads were resuspended in 20 μl TE buffer.

PCR with the teltail and P1 PCR primers was performed using Q5 PCR enzyme mix (NEB, M0494) and the following conditions using 0.1 μl DNA-bound beads: denaturation at 98 °C for 30 s; 30 cycles of 10 s at 98 °C, 20 s at 69 °C, and 50 s at 72 °C; final extension for 5 min at 72 °C. PCR products were denatured at 80 °C for 5 min in 2× loading buffer containing 95% formaldehyde, 10 mM EDTA, 0.05% xylene cyanol (Sigma, X4126), and 0.05% bromophenol blue (Sigma B-1256) and separated on 4.5% polyacrylamide/7 M urea gels in 1× TBE buffer and electroblotted in 0.5× TBE onto nylon membranes (Hybond-N$^+$, Cytiva). DNA was UV-crosslinked to the membranes, hybridized with γ-^{32}P-ATP end-labelled $[TTAGGG]_4$ (TelG probe) in Church mix at 48 °C overnight and washed 3 times in 4× SSC and 1 time in 4× SSC/0.1% SDS at 48 °C for 5 min each wash. Imaging was done with a Typhoon phosphorimager.

For PCR assay with synthetic telomeric oligonucleotides $[TTAGGG]_{5-20}$–TTAG-$[A]_{10}$, 20 pM single strand oligonucleotide DNA was used for primer extension. The poly(A) tailing, AluI digestion, and DNA size selection steps were skipped. The standard curve was generated using ImageJ v_2.0 and GraphPad Prism software (Dotmatics, ver.10).

Generation of the model telomere substrate

A model telomere substrate containing a 56 nt 3′ telomeric overhang was constructed using the telomeric DNA containing BglII/HindIII fragment from pSXneo1.6T_2AG_3[43]. To generate the 3′ overhang, 1 μM 5′-CTAACCCTAAGCTCTGCGACAT-3′ and 5′-GATCATGTCGCAGAGC$[TTAGGG]_{11}$-3′ were phosphorylated with T4 polynucleotide kinase, annealed, and incubated with 0.1 μM linear pSXneo1.6T_2AG_3. Ligation was done in the presence of BglII and HindIII with 6 cycles at 37 °C for 5 min and 21 °C for 5 min. The ligated product was gel purified on a 1% agarose gel.

ExoI digestion

Genomic DNA and the model telomere substrate were incubated with 40 U *E. coli* ExoI (M0293, NEB) in 67 mM Glycine-NaOH (pH 9.5), 6.7 mM $MgCl_2$ and 10 mM 2-mercaptoethanol at 37 °C for >6 h. After ExoI digestion, DNA was purified by PCI extraction and precipitated by adding 1/20 volume of 8 M LiCl and 1 volume of isopropanol. For in-gel and Southern blot telomere hybridization assays, genomic DNA was digested with MboI and AluI after the ExoI treatment.

Oligonucleotides for the PCR method

Oligonucleotides were synthesized by IDT or Thermo Fisher with indicated modifications and purification on polyacrylamide gel electrophoresis.

The teltail ss adaptors 1-6 used for extension were as follows (telomeric sequences underlined). Adaptor 1: 5′-[5biotin]- TGCTCCGTGC ATCTGGCATC TTTTTTTT CTAA−3′; adaptor 2: as adaptor 1 but ending in TAAC−3′; adaptor 3: as adaptor 1 but ending in AACC−3′; adaptor 4: as adaptor 1 but ending in ACCC−3′; adaptor 5: as adaptor 1 but ending CCCT−3′; adaptor 6: as adaptor 1 but ending in CCTA−3′.

The P1 ds-adaptors upper 1-6 oligonucleotides were as follows (telomeric sequences underlined). Upper 1: 5′-[5AmMC6]- GCACA GCCACTGGTAACG CCC GGTTAG-[3AmC7]−3′; upper 2, as upper 1 but ending in GTTAGG-[3AmC7]−3′; upper 3: as adaptor 1 but ending in TTAGGG-[3AmC7]−3′; upper 4: as adaptor 1 but ending in

TAGGGT-[3AmC7]–3′; upper 5: as adaptor 1 but ending in AGGGTT-[3AmC7]–3′; upper 6: as adaptor 1 but ending in GGGTTA-[3AmC7]–3′. The P1 ds-adaptor lower was: 5′-[5phos]-CGTTACCAGTGGCTGTGC-[3ddC]–3′.

PCR was performed with the following primers. Teltail primer: 5′-TGCTCCGTGCATCTGGCATC-3′; P1 primer: 5′-GCACAGCCACTGG TAACG-3′

The following control oligonucleotides were used to test the assay. Tel5-TTAG-A10: 5′-$[TTAGGG]_5$TTAG AAAAAAAAAA-3′; Tel10-TTAG-A10: 5′-$[TTAGGG]_{10}$TTAG AAAAAAAAAA-3′; Tel15-TTAG-A10: 5′-$[TTAGGG]_{15}$TTAG AAAAAAAAAA-3′; Tel20-TTAG-A10: 5′-$[TTAGGG]_{20}$ TTAG AAAAAAAAAA-3′.

Telomeric overhang measurement (method II)

In method II, genomic DNA isolated as described previously[44] was treated (or not) with *E. coli* ExoI as described above, digested with MboI and AluI, purified by PCI extraction, isopropanol precipitated, and resuspended in 2 mM Tris-HCl (pH 7.4) containing 0.2 mM EDTA. DNA (1.5 µg) was suspended in alkaline loading buffer containing 50 mM NaOH, 1 mM EDTA, 3% Ficoll 400 (Sigma, F9378), 0.5% (w/v) bromocresol green, 0.9% (w/v) xylene cyanol FF, fractionated on alkaline gels (0.7% agar, 50 mM NaOH and 1 mM EDTA) in alkaline running buffer contains 50 mM NaOH and 1 mM EDTA as described[44]. The gels were neutralized in neutralizing buffer (0.5 M Tris-HCl pH 7.0 and 3 M NaCl), dried and processed for in-gel overhang assays with end-labelled TelC as described above. Gels were scanned using a Typhoon phosphorimager, and the hybridization intensity of the scan was read and analysed using Fiji software (ImageJ v_2.0). The average size of the fragments was calculated taking into account that the hybridization intensity increases with fragment length[45]. To account for the subtelomeric component of the telomere restriction fragments (0.5 kb) the mean telomere restriction fragment length (TRF) was calculated as: mean TRF = $\Sigma(SI_i)/\Sigma\{SI_i/(MW_i - 0.5)\} + 0.5$, where SI_i is the signal intensity at position *i* and MW_i is the TRF length at that position. Overhang lengths were calculated by comparing the G-strand length before and after ExoI treatment.

As a control, pSXNeo1.6T_2AG_3[43] was digested with HindIII and BglII, ligated (or not) to an oligonucleotide bearing a telomeric 3′ overhang of 56 nt (as described above for the model telomere substrate), and the 3-kb fragments with and without the overhang were purified from agarose gel. The DNA fragments were treated (or not) with 20 U of *E. coli* ExoI, processed on alkaline gels as above, and detected by in-gel hybridization with the TelC probe.

DNA markers for telomere blotting

For telomere markers, pSXneo1.6T_2AG_3 was digested by following combinations of restriction enzymes (NEB), and fragments of the corresponding sizes were purified from 1% agarose TAE gel electrophoresis. 5,366 bp marker: BglII in NEB buffer r3.1; 4,470 bp: PvuII/BglII (r3.1); 2,965 bp: HindIII/BglII (r3.1); 887 bp: KpnI-HF in rCutSmart (rCS); 3,304 bp: PciI/NdeI (r3.1); 3,121 bp: HincII/NdeI (rCS); 2,814 bp: NaeI/NdeI (rCS); 2,616 bp: BsaI/NdeI/ScaI-HF (rCS); 3,213 bp: PciI/BglII (r3.1); 3,017 bp: HincII/NotI-HF (rCS); 2,710 bp: NaeI/NotI-HF/ScaI-HF (rCS); 2,512 bp: BsaAI/NotI-HF (rCS). DNA (10 pg) for each marker was loaded per lane for gel electrophoresis. Each fragment contains 1.5 kb telomeric repeat sequences, with the exception of the 887 bp KpnI-HF fragment which contains 0.8 kb telomeric repeats. The markers were detected by hybridization to the TelC probe. For the detection of the 1 kb DNA ladder (NEB, N3232) and the λ HindIII/φX HaeIII marker, DNA ladders were denatured, end-labelled using γ-^{32}P-ATP, and used as probes. Standard curves of the DNA markers were generated using GraphPad Prizm software (v_10.0) and the equation of the standard curve was generated using https://mycurvefit.com.

Alkaline gel analysis of the telomeric G- and C-strands

Genomic DNA from was digested with MboI and AluI and denatured in 50 mM NaOH and 1 mM EDTA before fractionating the DNA on 0.7% alkaline agarose gels as described above. Gels were neutralized in 0.5 M Tris-HCl (pH 7.0)/3 M NaCl, dried, prehybridized in Church mix for 1 h at 50 °C, and hybridized overnight at 50 °C in Church mix with γ-^{32}P-ATP end-labelled $[AACCCT]_4$ (TelC) or $[TTAGGG]_4$ (TelG) as described[10].

Statistics and reproducibility

The experiments in Fig. 1d,e and Extended Data Figs. 2e and 3e were performed a minimum of three times. For all other experiments, the number of replicates and statistics are indicated in the figures and figure legends.

Reporting summary

Further information on research design is available in the Nature Portfolio Reporting Summary linked to this article.

Data availability

All data are presented in Figs. 1–4 and Extended Data Figs. 2–9.

41. Guilliam, T. A. & Yeeles, J. T. P. Reconstitution of translesion synthesis reveals a mechanism of eukaryotic DNA replication restart. *Nat. Struct. Mol. Biol.* **27**, 450–460 (2020).
42. Komura, J. & Riggs, A. D. Terminal transferase-dependent PCR: a versatile and sensitive method for in vivo footprinting and detection of DNA adducts. *Nucleic Acids Res.* **26**, 1807–1811 (1998).
43. Hanish, J. P., Yanowitz, J. L. & de Lange, T. Stringent sequence requirements for the formation of human telomeres. *Proc. Natl Acad. Sci. USA* **91**, 8861–8865 (1994).
44. Smogorzewska, A., Karlseder, J., Holtgreve-Grez, H., Jauch, A. & de Lange, T. DNA ligase IV-dependent NHEJ of deprotected mammalian telomeres in G1 and G2. *Curr. Biol.* **12**, 1635–1644 (2002).
45. Harley, C. B., Futcher, A. B. & Greider, C. W. Telomeres shorten during ageing of human fibroblasts. *Nature* **345**, 458–460 (1990).

Acknowledgements The authors thank C. Price for providing the *CTC1*$^{fl/fl}$ HCT116 cell line; members of the de Lange laboratory for comments on this work; V. Risca and A. Mansisidor for advice on the PCR method; J. C. Zinder for the CTC1 antibody; and S. Cai for purified human RPA. This work is supported by grants from the NCI (R35CA210036), the NIA (RO1AG016642), and the BCRF to T.d.L.; a grant from the NCI to H.T. (5R50CA243771-02); and a grant to J.T.P.Y. from the Medical Research Council (no. MC_UP_1201/12).

Author contributions H.T. and T.d.L. conceived and designed the study. V.A. and J.T.P.Y. designed and performed the in vitro replication experiments. All in vivo experiments were executed by H.T. with help from P.B. in the early stages of the project. T.d.L. and J.T.P.Y. wrote the manuscript with input from all authors.

Competing interests The authors declare no competing interests.

Additional information

Supplementary information The online version contains supplementary material available at https://doi.org/10.1038/s41586-024-07137-1.

Correspondence and requests for materials should be addressed to Joseph T. P. Yeeles or Titia de Lange.

Peer review information *Nature* thanks Joachim Lingner and the other, anonymous, reviewer(s) for their contribution to the peer review of this work. Peer review reports are available.

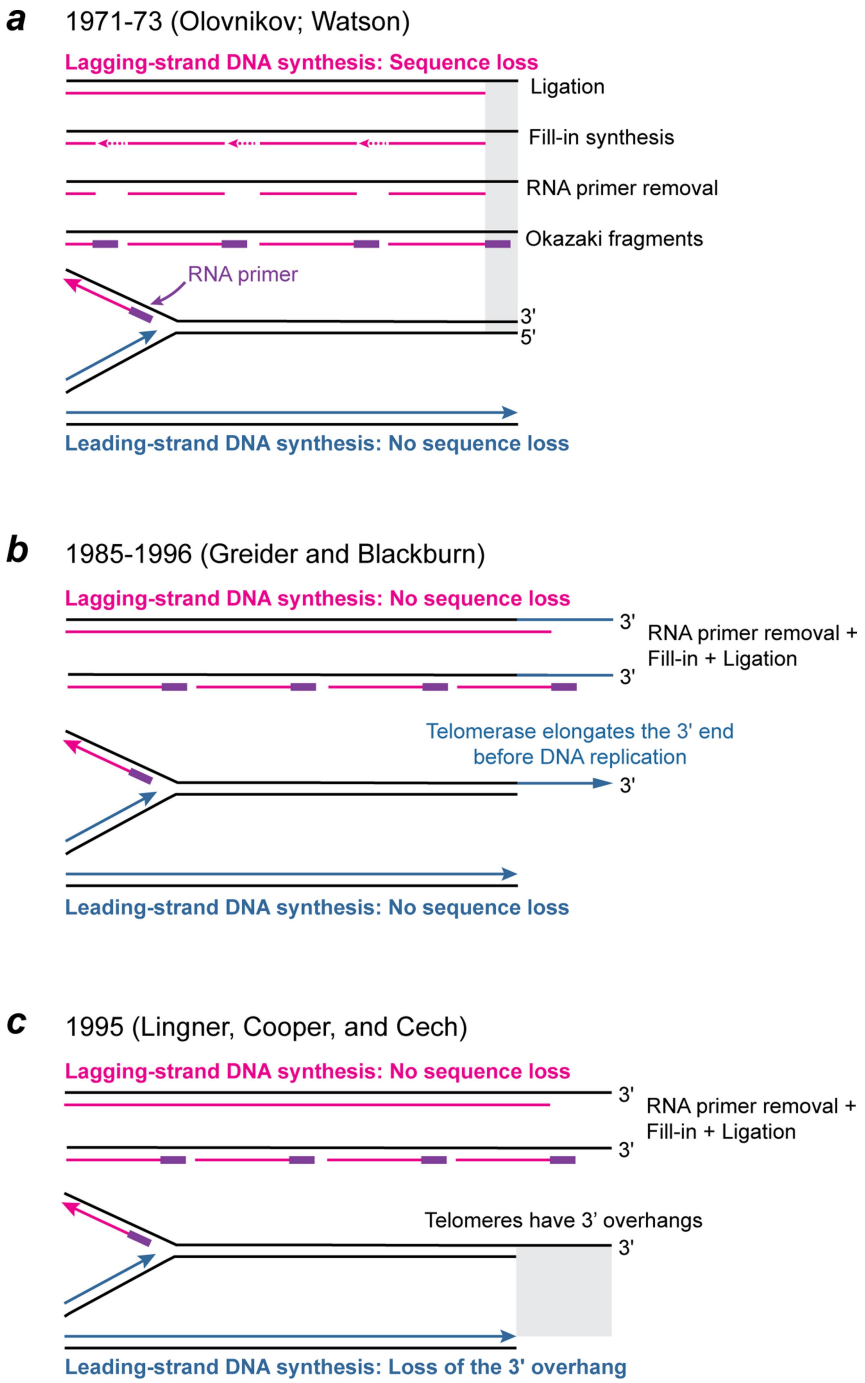

Extended Data Fig. 1 | Changing views of the end-replication problem. **a**, The first version of the end-replication problem as perceived by Watson[5] and Olovnikov[6] after it was shown that Okazaki fragments carry RNA primers at their 5′ ends. In this end-replication problem, the 5′ ended strand of the lagging-strand DNA synthesis product is shorter than the parental strand. **b**, Telomerase was suggested to solve the end-replication problem by extending the 3′ ends before DNA replication[7]. **c**, When it had become clear that telomeres ended in a 3′ overhang, it was argued that the end-replication problem involved the inability of leading-strand DNA synthesis to recreate this part of the telomeric DNA[2]. Therefore, the end-replication problem involved the shortening of the G-rich strand at leading-end telomeres. Telomerase can solve the leading-end replication problem by acting after DNA replication (and 5′ end resection) as shown in Fig. 1a. If the last Okazaki fragments start on the 3′ overhang (as shown), no sequence loss will occur at lagging-end telomeres. The end-replication problem was therefore "no longer a lagging strand problem" (quote from ref. 2).

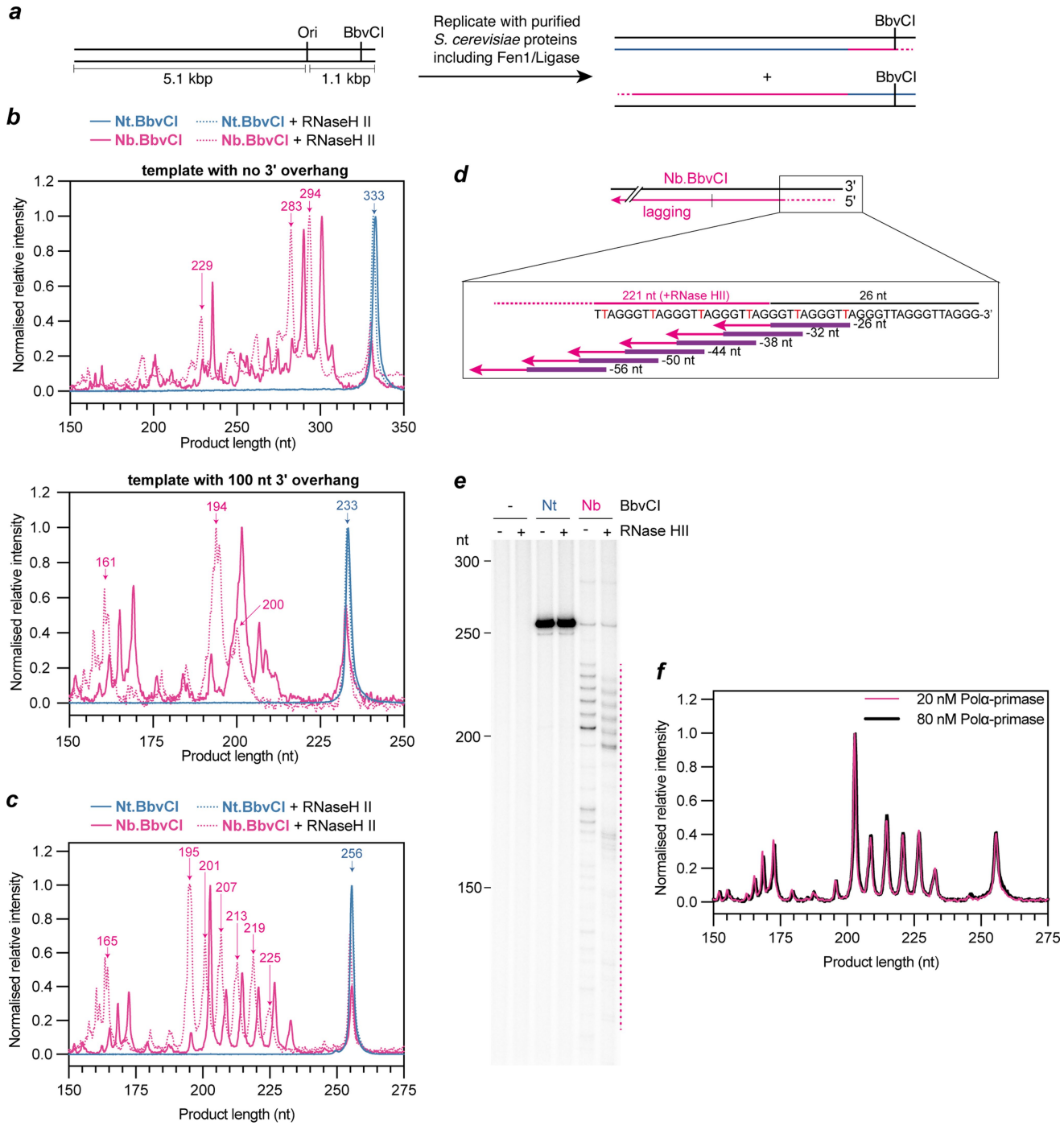

Extended Data Fig. 2 | Analysis of replisome-mediated DNA synthesis at the end of linear DNA templates. a, Schematic of the replication templates used for in vitro budding yeast DNA replication and the anticipated reaction products of origin-dependent replication. **b** and **c**, Analysis of the data presented in Fig. 1d (**b**) and 1f (**c**). Product length was determined using a standard curve derived from the molecular weight standards. Replication product intensity was normalised by dividing each data point by the amplitude of the most intense product for a given condition. **d**, Schematic illustrating the terminal TTAGGG repeats that are used to initiate Okazaki fragment synthesis during in vitro DNA replication. **e**, Replication reaction performed and analyzed as in Fig. 1f but with the concentration of Polα-primase increased from 20 nM to 80 nM. To enable clear visualization of the Nb.BbvCI products, the Nt.BbvCI product bands are saturated. **f**, Comparison of Nb.BbvCI digested replication products in the absence of RNase HII at 20 nM (Fig. 1d) and 80 nM (**e**) Polα-primase. Data were processed as described for (**b**) and (**c**).

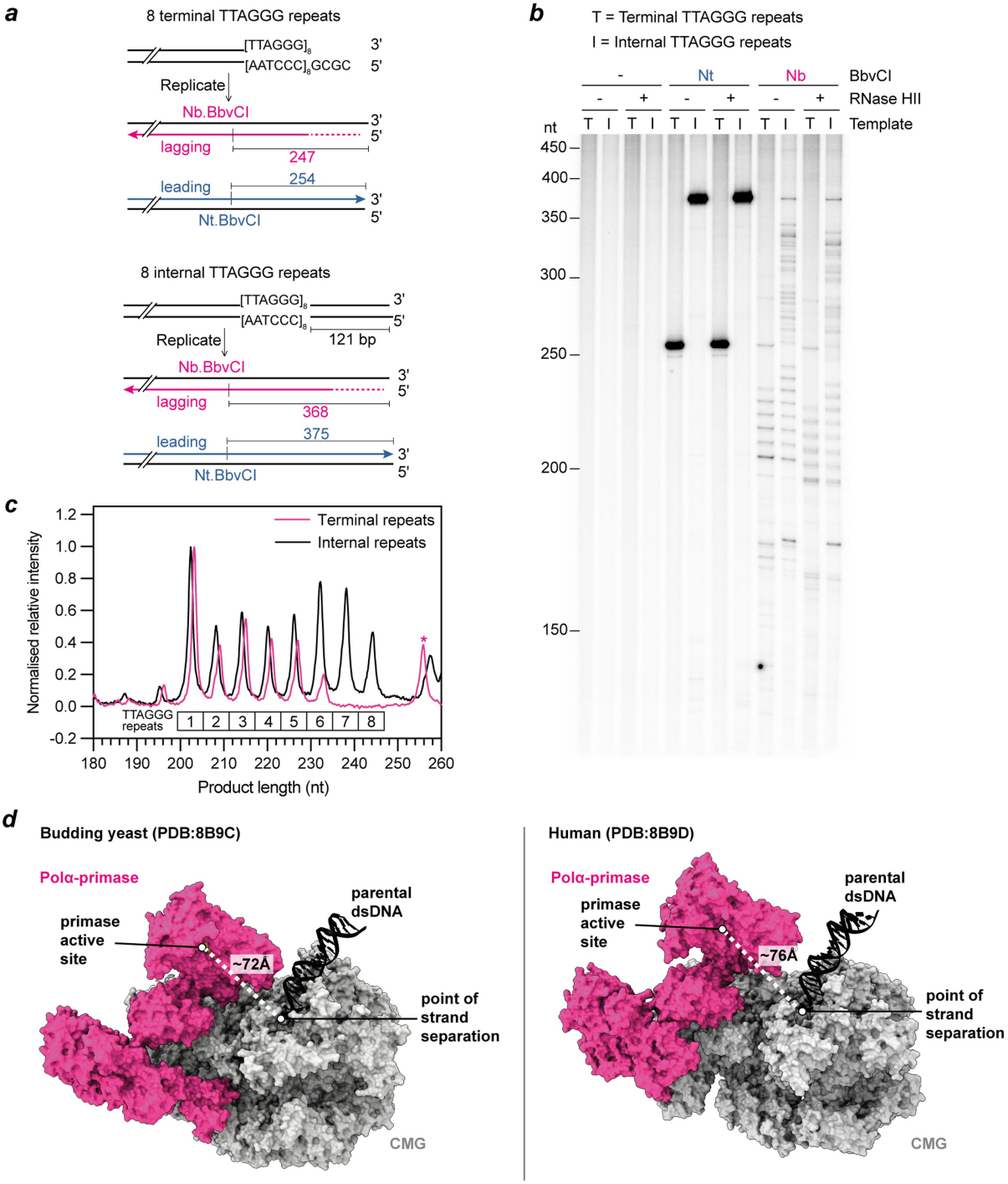

Extended Data Fig. 3 | Analysis of lagging-strand priming within TTAGGG repeats. a, Schematic illustrating the TTAGGG repeat containing templates and the anticipated products of Nt./Nb.BbvCI digestion. By linearizing the plasmids with different restriction enzymes, the TTAGGG repeats are located either at the end of the template, or 121 bp from the end of the template. **b**, Denaturing 5% polyacrylamide/urea gel analysis of a replication reaction on the templates shown in (**a**) analyzed as described in Fig. 1d. To enable clear visualization of the Nb.BbvCI products, the Nt.BbvCI product bands are saturated. **c**, Comparison of Nb.BbvCI digested replication products in the absence of RNase HII from (**b**). The asterix marks the presence of an RNase HII insensitive replication product. The position of the template strand TTAGGG repeats are illustrated below the traces. **d**, Comparison of Polα-primase in the yeast and human replisomes (from reference[19]). For clarity only Polα-primase (pink), the CMG helicase (grey) and DNA (black) are shown. The shortest distance between the point of strand separation and the primase active site are illustrated (dashed white lines).

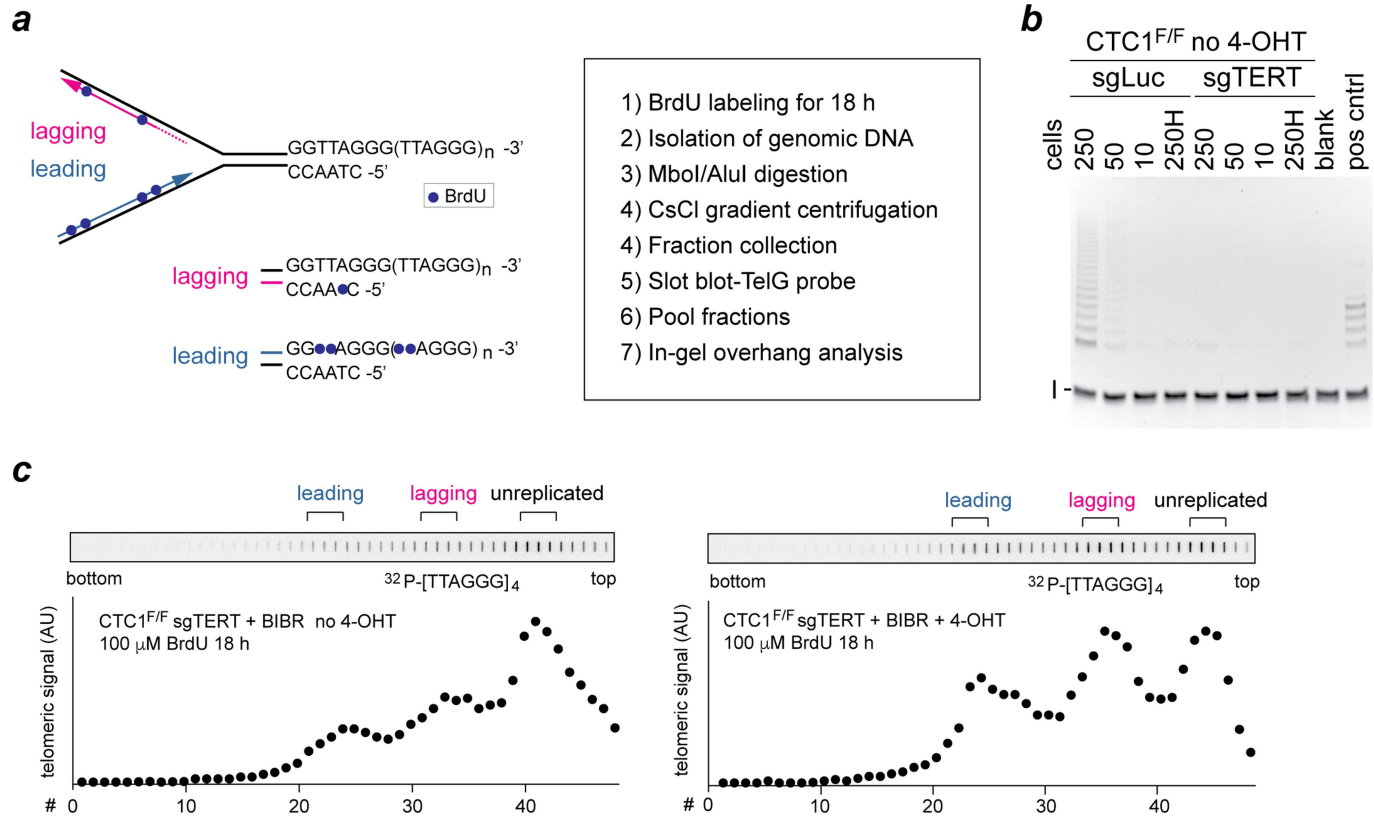

Extended Data Fig. 4 | CsCl-gradient separation of leading- and lagging-end telomeres from CTC1$^{F/F}$ cells lacking telomerase activity. a, Schematic of the experimental approach to separate telomeres replicated by leading- and lagging-strand DNA synthesis. **b**, TRAP assay on extracts from CTC1$^{F/F}$ cells from which hTERT is deleted (in bulk) using CRISPR/Cas9 (sgTERT). Cells treated with a Luciferase sgRNA are used as the control. Cell equivalents are indicated above the lanes. 250H: Heat-inactivated extract (250 cells). Positive control sample (pos cntrl) provided by the manufacturer. I: internal PCR control. **c**, Examples of slot blots to detect telomeric DNA in fractions from CsCl gradients. Pooled fractions used for in gel 3′ overhang assays are indicated at the top.

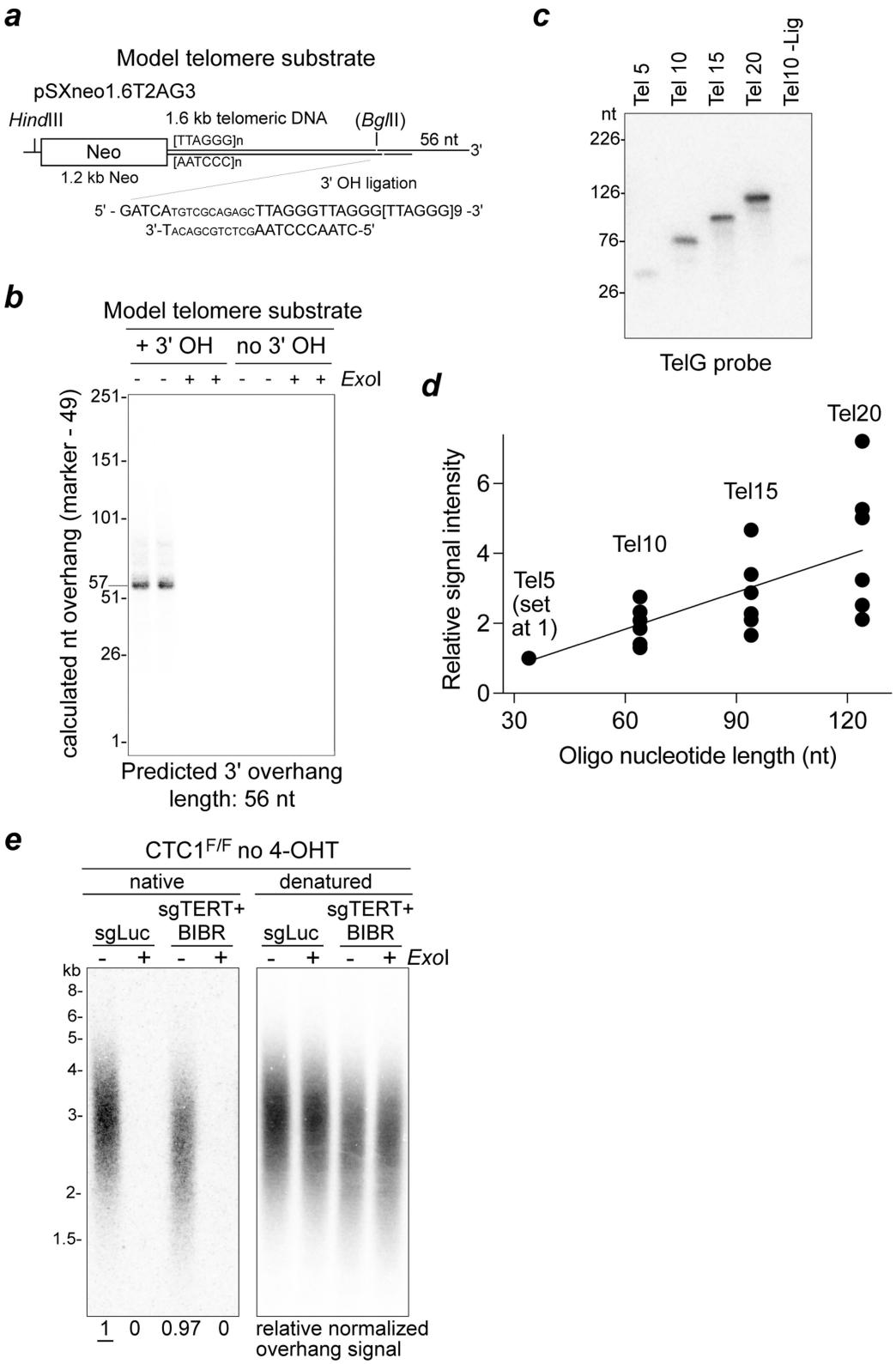

Extended Data Fig. 5 | Validation of the PCR overhang assay (Method I). **a**, Schematic of the telomere model substrate generated by ligating a telomeric 3′ overhang to a HindIII/BglII fragment of pSXneo1.6T_2AG_3. **b**, PCR overhang assay on the model telomeric substrate before and after *E. coli* 3′ exonuclease ExoI treatment to remove the 3′ overhang. **c**, PCR overhang assays performed with synthetic telomeric oligos containing 5 to 20 TTAGGG repeats. Tel10 -Lig: Tel10 oligo processed in parallel but without ligation to the adaptor. **d**, Relative signal intensity of 6 independent PCR overhang assays as in (**c**) were plotted. The signal intensity of Tel5 oligo in each experiment was set at 1. **e**, In-gel hybridization assay showing that telomerase expression does not strongly alter 3′ overhang lengths when CTC1-profient cells and that the ExoI digestion used in Fig. 2e worked. Genomic DNAs from $CTC1^{F/F}$ cells with or without sgTERT and BIBR1532 treatment were treated with *E. coli* ExoI as indicated and digested with MboI/AluI for the in-gel overhang assay shown. Left: TelC probe detecting the overhang signals. Right: same gel probed with TelC after in situ denaturation to detect the total telomeric DNA for normalization.

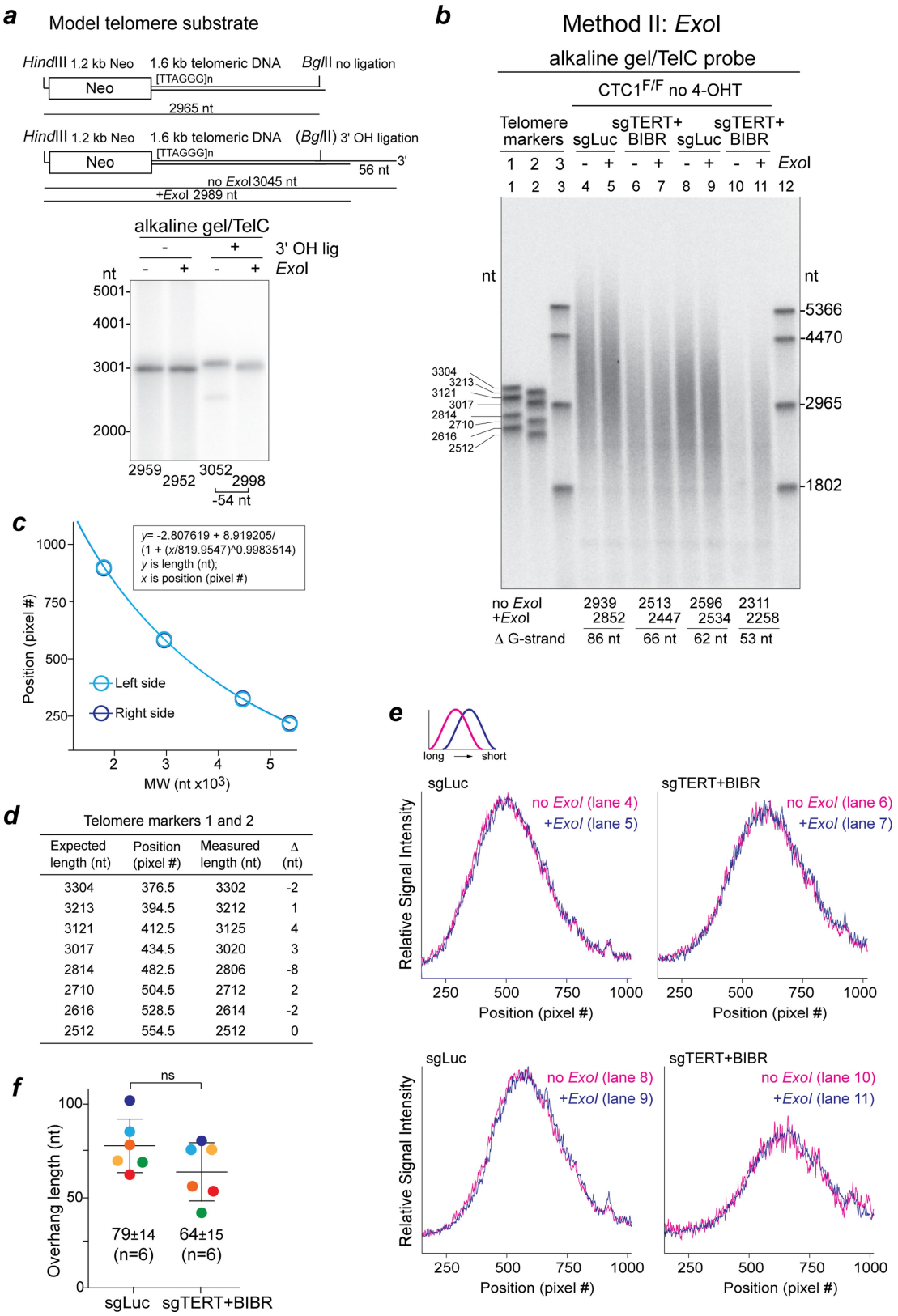

Extended Data Fig. 6 | See next page for caption.

Extended Data Fig. 6 | Overhang measurement with ExoI digestion (Method II). a, Top: Telomere model substrate with or without overhang (as in Extended Data Fig. 5a) with predicted fragment lengths indicated. Bottom: Telomere model substrate with and without overhang was treated with or without ExoI, separated by alkaline agarose gel electrophoresis and detected by in-gel hybridization with the TelC probe. Sizes of the detected fragments were calculated based on the molecular weight marker. Shortening of the model telomere substrate G-strand by ExoI is shown below the gel. **b**, Example of determination of G-strand shortening by ExoI treatment. DNAs from cells with or without depletion of telomerase (sgTERT+BIBR) were treated with ExoI as indicated and subsequently digested with MboI and AluI. DNAs were separated on an alkaline agarose gel and the gel was dried and hybridized with TelC. Changes in G-strand length after ExoI treatment are indicated below the lanes. The MW markers are generated by restriction digestion of pSXneo1.6T2AG3 (see Extended Data Fig. 5a and Methods) and fragments containing TTAGGG repeats are detected with TelC. **c**, Graph of migration (pixel position) versus the MW of the telomeric marker in lane 3 and lane 12 of the gel in (**b**) generated by scanning of the gel using Fiji software (ImageJ, ver2.0). The equation of the curve is used to convert migration (pixel #) to telomere lengths. **d**, Measured lengths of the telomere markers in lane 1 and 2 was calculated using the position of the fragment (pixel #) in the gel and the equation generated from standard curve in (**c**) and compared to the expected length. **e**, Overlay of the scan profiles of G-strand telomeric signal from DNA treated with or without ExoI shown in (**b**). Line graphs shift to the right (lower MW) in DNAs treated with ExoI compared to mock-treated DNAs. **e**, Graph showing average 3′ overhang lengths and SDs determined by Method II on 6 biological replicates. ns, not significant based on unpaired two-sided t-test.

a

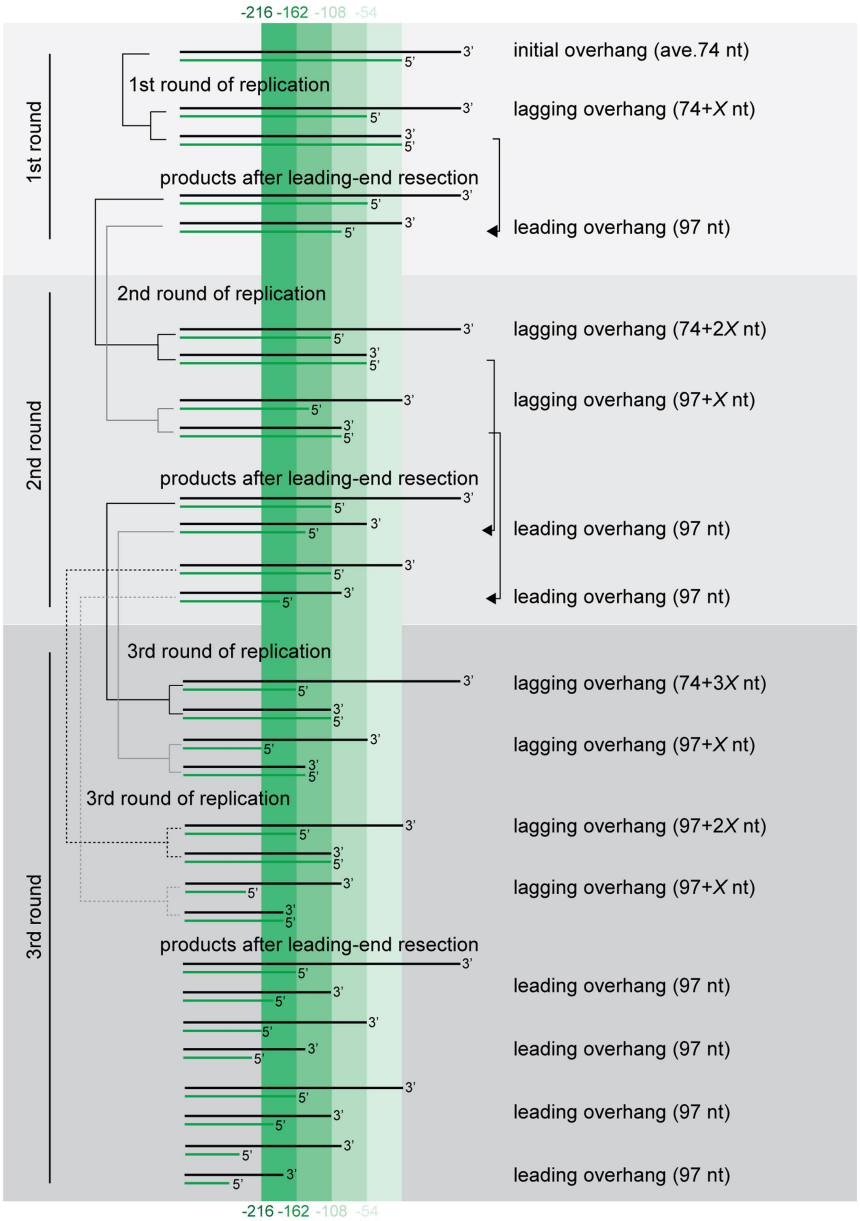

b

$$\frac{F_{lag} + R_{lead}}{2} = \frac{(2^{D\#} - 1)X + Y + (2^{D\#} - 1)R_{lead}}{2^{D\#}}$$

When *D#*=5 and F_{lag} =201, *X*=54.4

Y = initial overhang length (74 nt)
D# = rounds of replication
R_{lead} = resection at leading ends (97 nt)
F_{lag} = length of lagging OH after *D#*
X = loss at lagging end/cell division

c

Predicted 3' overhang length		
lagging strand	leading strand	average
1st round: 128 nt	1st round: 97 nt	1st round: 113 nt
2nd round: 167 nt	2nd round: 97 nt	2nd round: 132 nt
3rd round: 186 nt	3rd round: 97 nt	3rd round: 142 nt
4th round: 196 nt	4th round: 97 nt	4th round: 147 nt
5th round: 201 nt	5th round: 97 nt	5th round: 149 nt

Extended Data Fig. 7 | See next page for caption.

Extended Data Fig. 7 | Calculation of C-strand shortening at lagging-end telomeres. a and **b**, Calculation of the C-strand loss at lagging-end telomeres in cells lacking CTC1 and telomerase activity. The schematic in (**a**) shows the changes at leading- and lagging-end telomeres over three rounds of replication assuming 97 nt (average of 110 and 84 nt) resection of the leading-end products as determined in Fig. 2i. Sequence loss at the lagging-end C-strand is calculated to be 54 nt based on the 3′ overhang length of 201 nt (average of 228 and 173) for lagging-end telomeres after 5 divisions without CTC1 (Fig. 2i) and applying the equation in (**b**). Note that the 97 nt loss at the leading-end telomeres is constant, whereas the loss at the lagging-end telomeres increases with each division. **c**, Predicted overhang length changes in 5 successive rounds of replication after *CTC1* deletion from telomerase-deficient cells as depicted in (**a**). Note that the value for the lagging-end overhangs is predicted to plateau (at ~205 nt) while the leading-end overhangs are constant at 97 nt. Therefore, the average overhang length is predicted to plateau at ~150 nt which represents a doubling of the length (starting length 74 nt before CTC1 deletion) consistent with the two-fold increase in the relative overhang signal observed in Fig. 3c.

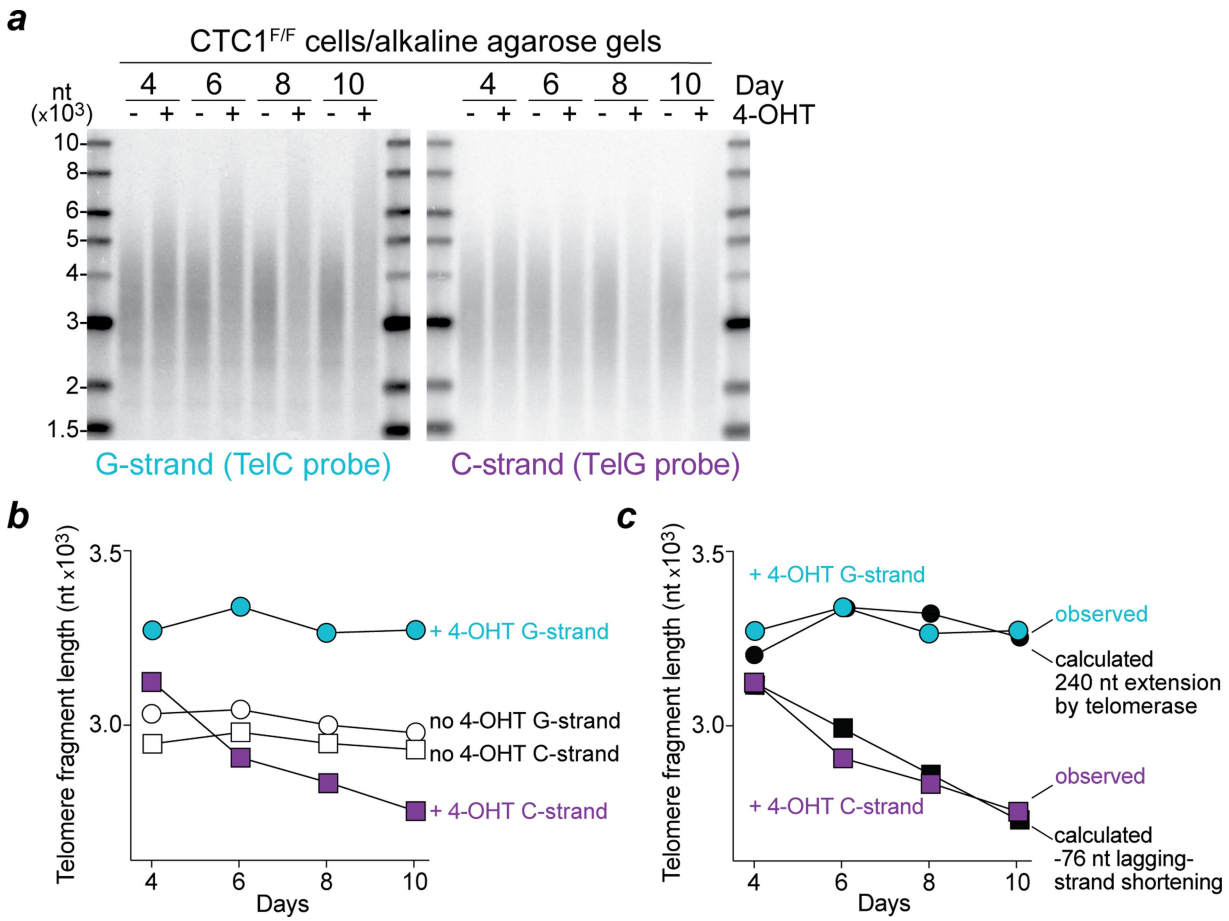

Extended Data Fig. 8 | C-strand shortening in HCT116 cells lacking CTC1. a–c, Measurement of C-strand shortening CTC1$^{F/F}$ cells with or without 4-OHT treatment based on alkaline gel analysis of the telomeric G- and C-strands as in Fig. 4b–d.

a

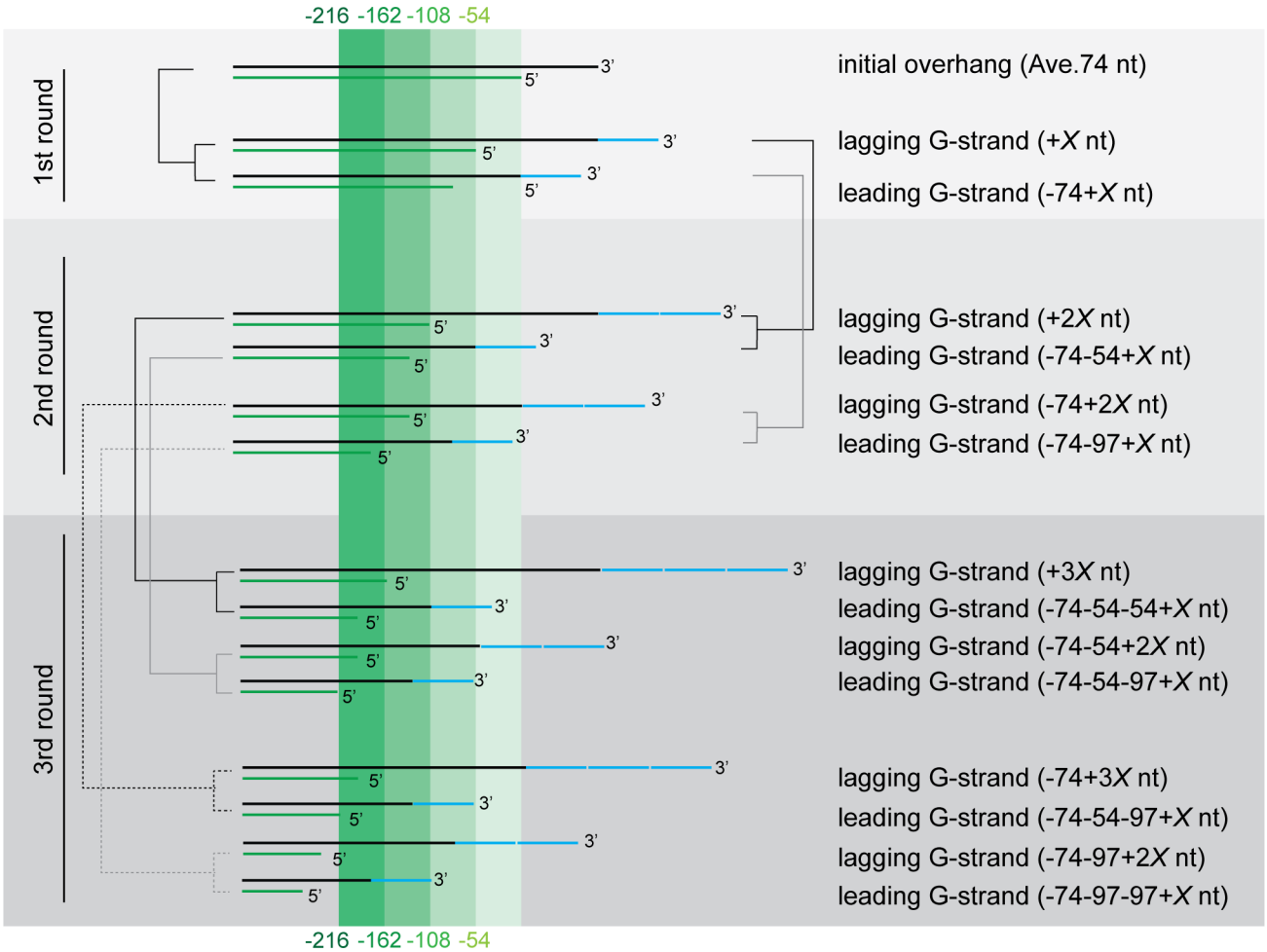

b

$$\frac{1}{2^n}\sum_{k=1}^{n}\{[-Y-\frac{Rlag+Rlead}{2}(k-1)]2^{k-1}+2^kX\}$$

n: number of cell divisions
Rlag: C-strand shortening at lagging strands ends (54 nt)
Rlead: C-strand shortening at leading strands ends (97 nt)
Y: initial 3' overhang length (74 nt)
X: G-strand elongation by telomerase (nt/cell division)

c

Average change in G-strand length after the indicated rounds of replication w/o Ctc1 (assuming *X*=240 nt/division)	
1st round:	+203 nt
2nd round:	+267 nt
3rd round:	+261 nt
4th round:	+220 nt
5th round:	+161 nt

d

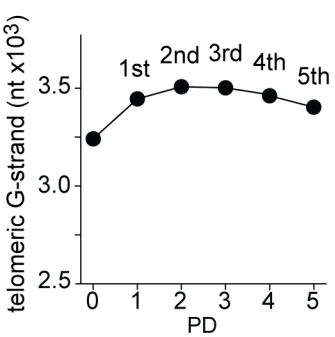

Extended Data Fig. 9 | Schematic illustrating the dynamics of the C- and G-strand in CTC1-deficient cells expressing telomerase. a, Schematic showing the changes of G- and C-strand telomere length over three rounds of replication in telomerase-proficient cells lacking CTC1. G-strand sequences added by telomerases are depicted with a blue line. The numbers given are as follows (based on Fig. 2i,j). *X*: nucleotides added by telomerase; 74 nt: initial 3′ overhang length; 54 nt: loss of sequences due to incomplete lagging-strand synthesis; 97 nt: loss of sequences due to resection of the C-strand at leading-end telomeres. **b**, Equation describing changes in average G-strand length after each round of replication (n) relative to initial G-strand telomere length. **c**, Increase in average G-strand length with cell divisions calculated using the equation in (**b**) and assuming that telomerase adds an average of 240 nt (*X*) to each end. **d**, Modeled changes in the length of the G-strand in Ctc1-deficient cells based on the initial G-strand length of 3.24 kb. To determine *X*, the value for telomerase extension was increased stepwise by 10 nt, plotted and the plot was compared to the actual G-strand changes obtained in Fig. 4d. When *X* is 240 nt, the model plot is a close fit with the in vivo rate of G-strand elongation in Fig. 4d.

nature portfolio

https://doi.org/10.1038/s41586-024-07137-1

Supplementary information

CST–polymerase α-primase solves a second telomere end-replication problem

In the format provided by the authors and unedited

SUPPLEMENTARY INFORMATION GUIDE

CST–Polymeraseα-primase solves a second telomere end-replication problem

Hiroyuki Takai**, Valentina Aria**, Pamela Borges, Joseph T. P. Yeeles*, Titia de Lange*

*Corresponding authors: Joseph T. P. Yeeles: jyeeles@mrc-lmb.cam.ac.uk and Titia de Lange: delange@rockefeller.edu
** equal contribution

Supplementary Figure 1. Uncropped images of blots for Figures 1-4 and Extended Data Figures 3-6 and 8

Source Data is provided as separate files.

Supplementary Information Figure 1: uncropped blots from Takai, Aria et al.

Fig. 1d

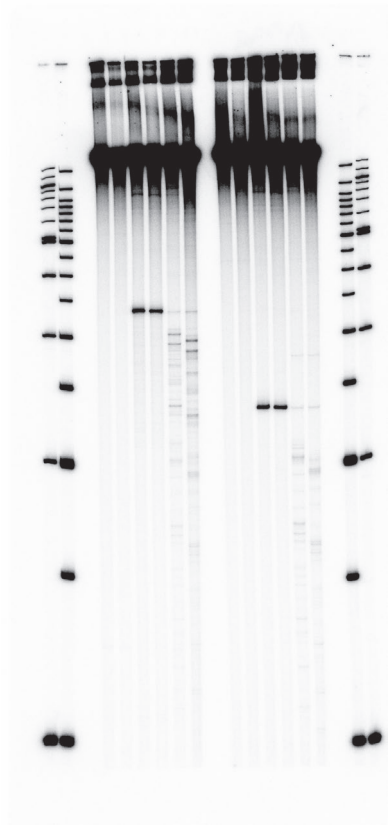

Fig. 1f and Ext Data Fig. 2e

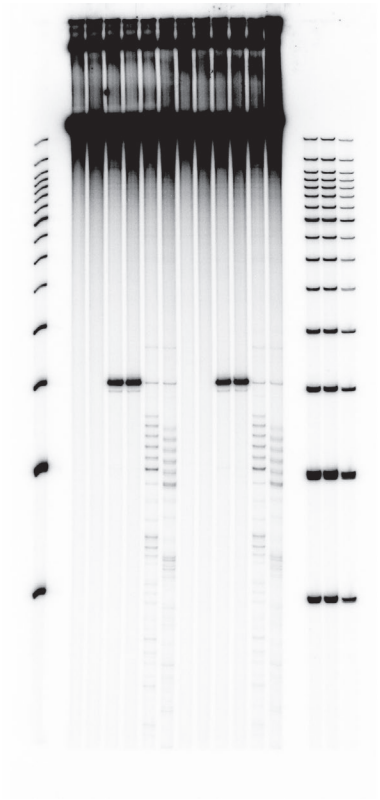

Fig. 2a

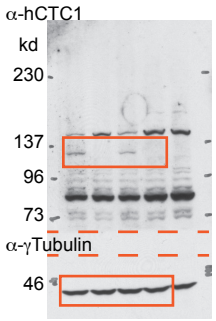

Membrane was cut between 73 kd and 46 kd markers

Fig. 2b

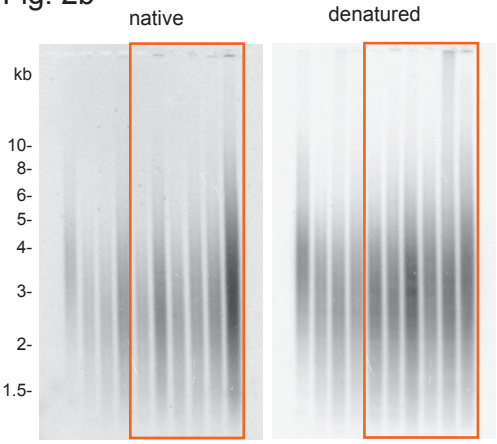

Fig. 2g

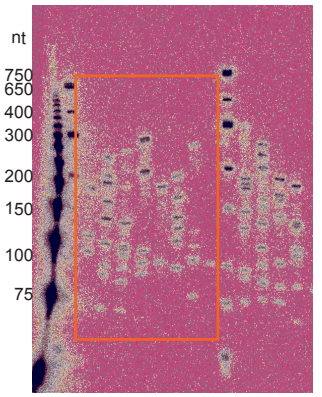

Fig. 2e

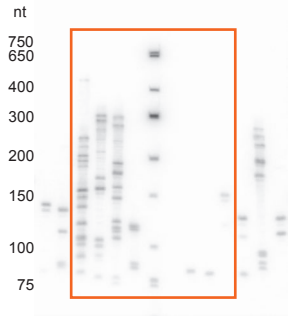

Fig. 2f

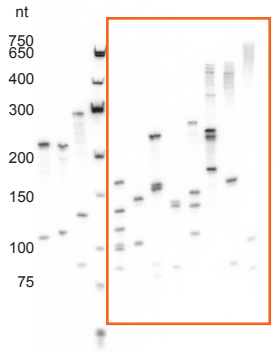

Fig. 2e,g,f show the images before the hybridization with size marker.

Fig. 3b

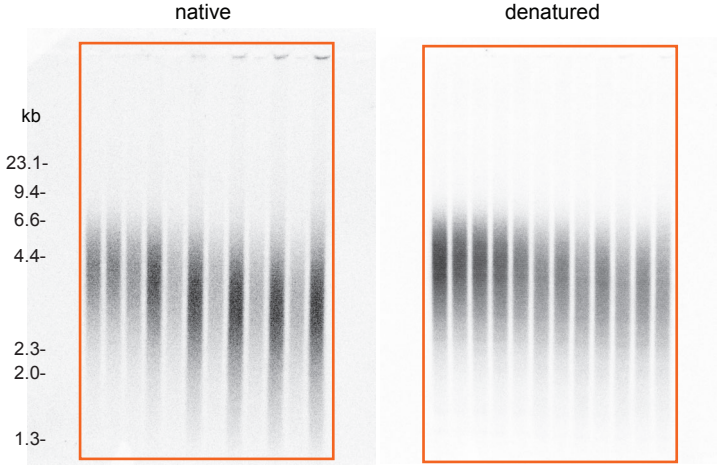

Fig. 4a

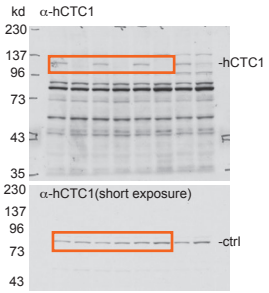

Fig. 4b

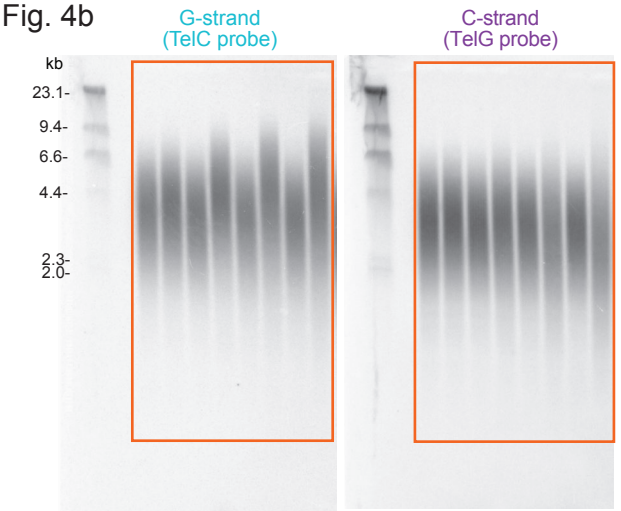

Supplementary Figure 1

Ext Data Fig. 3b

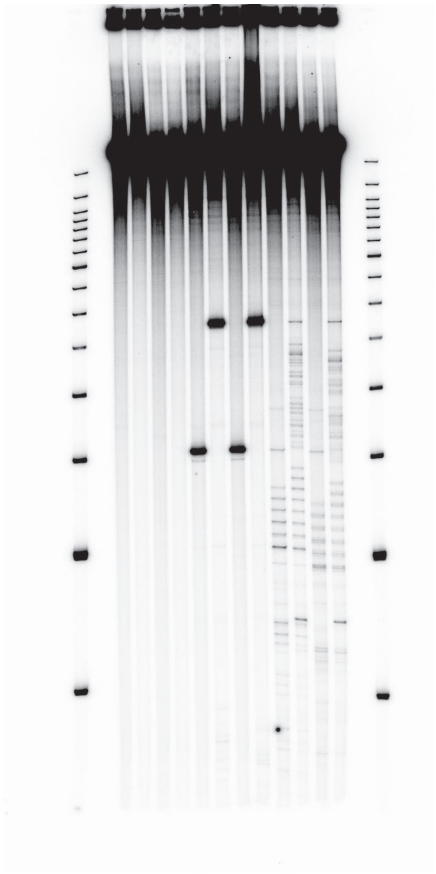

Ext Data Fig. 5b

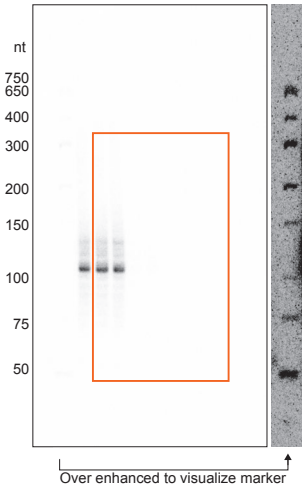

Ext Data Fig. 5c

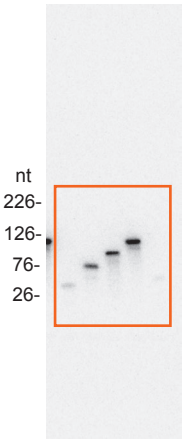

Ext Data Fig. 5e

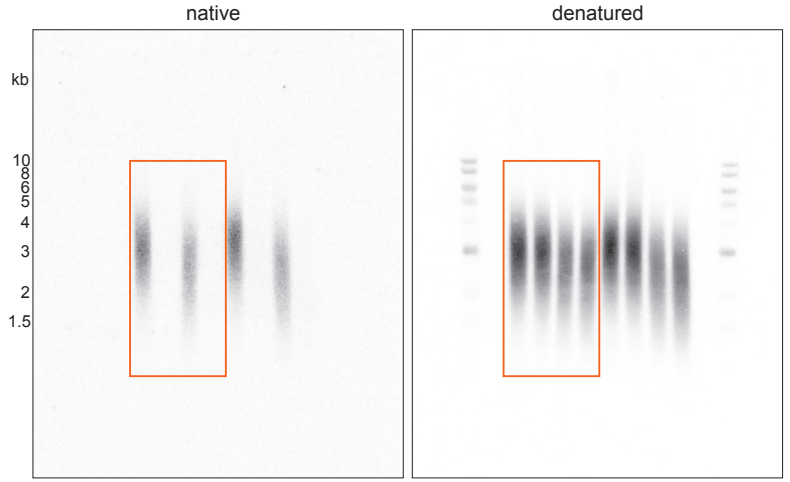

Ext Data Fig. 6a

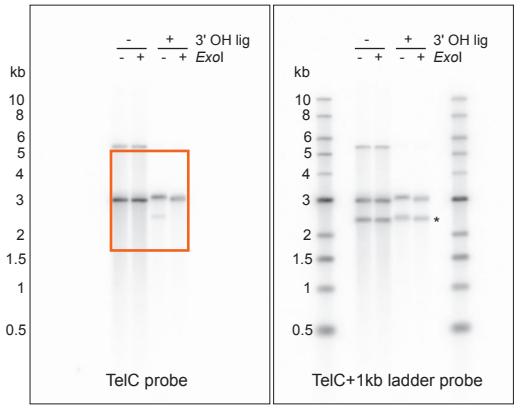

Image shown in Ext. Data Fig. 6a is before the gel was hybridized with 1 kb ladder probe.

*; cross-reaction from 1 kb ladder probe hybridization.

Ext Data Fig. 6b

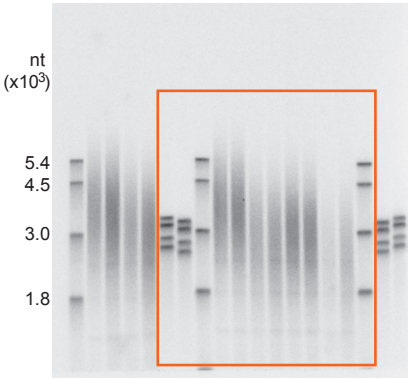

Ext Data Fig. 4b

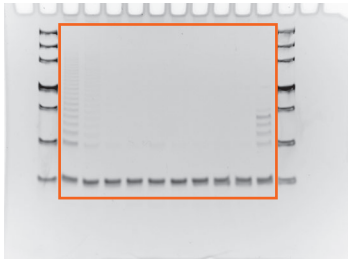

Ext Data Fig. 8a

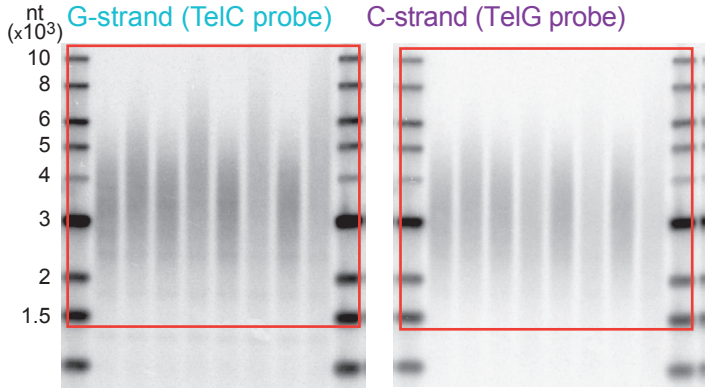

nature portfolio

Corresponding author(s): Joseph PT Yeeles and Titia de Lange

Last updated by author(s): 2024 01 09

Reporting Summary

Nature Portfolio wishes to improve the reproducibility of the work that we publish. This form provides structure for consistency and transparency in reporting. For further information on Nature Portfolio policies, see our Editorial Policies and the Editorial Policy Checklist.

Statistics

For all statistical analyses, confirm that the following items are present in the figure legend, table legend, main text, or Methods section.

n/a	Confirmed
☐	☒ The exact sample size (*n*) for each experimental group/condition, given as a discrete number and unit of measurement
☐	☒ A statement on whether measurements were taken from distinct samples or whether the same sample was measured repeatedly
☐	☒ The statistical test(s) used AND whether they are one- or two-sided *Only common tests should be described solely by name; describe more complex techniques in the Methods section.*
☒	☐ A description of all covariates tested
☐	☒ A description of any assumptions or corrections, such as tests of normality and adjustment for multiple comparisons
☐	☒ A full description of the statistical parameters including central tendency (e.g. means) or other basic estimates (e.g. regression coefficient) AND variation (e.g. standard deviation) or associated estimates of uncertainty (e.g. confidence intervals)
☐	☒ For null hypothesis testing, the test statistic (e.g. *F*, *t*, *r*) with confidence intervals, effect sizes, degrees of freedom and *P* value noted *Give P values as exact values whenever suitable.*
☒	☐ For Bayesian analysis, information on the choice of priors and Markov chain Monte Carlo settings
☒	☐ For hierarchical and complex designs, identification of the appropriate level for tests and full reporting of outcomes
☒	☐ Estimates of effect sizes (e.g. Cohen's *d*, Pearson's *r*), indicating how they were calculated

Our web collection on statistics for biologists contains articles on many of the points above.

Software and code

Policy information about availability of computer code

Data collection	Amersham Typhoon scanner control v1.1.0.7
Data analysis	Amersham Typhoon scanner control v1.1.0.7, including ImageQuant, Prism GraphPad v_10.0 and Dotmatics, v_1.0, Microsoft Excel v16.8, ImageJ 1.53a, Image J v_2.0, and mycurvefit.com for visualization

For manuscripts utilizing custom algorithms or software that are central to the research but not yet described in published literature, software must be made available to editors and reviewers. We strongly encourage code deposition in a community repository (e.g. GitHub). See the Nature Portfolio guidelines for submitting code & software for further information.

Data

Policy information about availability of data

All manuscripts must include a data availability statement. This statement should provide the following information, where applicable:

- Accession codes, unique identifiers, or web links for publicly available datasets
- A description of any restrictions on data availability
- For clinical datasets or third party data, please ensure that the statement adheres to our policy

All data supporting the findings of this study are available in the main figures, the extended data figures, and the Supplementary Information.

Research involving human participants, their data, or biological material

Policy information about studies with human participants or human data. See also policy information about sex, gender (identity/presentation), and sexual orientation and race, ethnicity and racism.

Reporting on sex and gender	n/a
Reporting on race, ethnicity, or other socially relevant groupings	n/a
Population characteristics	n/a
Recruitment	n/a
Ethics oversight	n/a

Note that full information on the approval of the study protocol must also be provided in the manuscript.

Field-specific reporting

Please select the one below that is the best fit for your research. If you are not sure, read the appropriate sections before making your selection.

☒ Life sciences ☐ Behavioural & social sciences ☐ Ecological, evolutionary & environmental sciences

For a reference copy of the document with all sections, see nature.com/documents/nr-reporting-summary-flat.pdf

Life sciences study design

All studies must disclose on these points even when the disclosure is negative.

Sample size	Sample size was determined based on prior published data from similar experiments (including data from our lab) e.g. PMID: 30451148, PMID: 22748632 and PMID: 27013236
Data exclusions	No data was excluded with the exception of data from failed experiments (e.g. sample loss; failure of Cre-mediated deletion; cell culture anomalies).
Replication	Every experiment reported was done at least three times with consistent results.
Randomization	Our analysis did not require randomization because it did not involve human subjects or live animals.
Blinding	Our analysis did not require blinding because it did not involve human subjects or live animals.

Reporting for specific materials, systems and methods

We require information from authors about some types of materials, experimental systems and methods used in many studies. Here, indicate whether each material, system or method listed is relevant to your study. If you are not sure if a list item applies to your research, read the appropriate section before selecting a response.

Materials & experimental systems

n/a	Involved in the study
☐	☒ Antibodies
☐	☒ Eukaryotic cell lines
☒	☐ Palaeontology and archaeology
☒	☐ Animals and other organisms
☒	☐ Clinical data
☒	☐ Dual use research of concern
☒	☐ Plants

Methods

n/a	Involved in the study
☒	☐ ChIP-seq
☒	☐ Flow cytometry
☒	☐ MRI-based neuroimaging

Antibodies

Antibodies used	Polyclonal rabbit anti-human CTC1 (a gift from John C. Zinder) at 1:3,000; monoclonal mouse anti human γtubulin (GTU-88, Sigma) at 1:10,000

Validation	The CTC1 antibody was validated by western blots of wild-type and CTC! CRISPR/Cas9 KO cells

Eukaryotic cell lines

Policy information about cell lines and Sex and Gender in Research

Cell line source(s)	Human conditional CTC1 KO HCT116 cells were described and provide by Dr. Price (Feng, X., Hsu, S. J., Kasbek, C., Chaiken, M. & Price, C. M. CTC1-mediated C-strand fill-in is an essential step in telomere length maintenance. Nucleic Acids Res 45, 4281-4293 (2017)).
Authentication	The cell line was verified based on tCre induced loss of Ctc1 in Western blots and telomeric phenotypes expected based on the Feng et al. publication cited above.
Mycoplasma contamination	No mycoplasma contaminations were found in the course of these experiments.
Commonly misidentified lines (See ICLAC register)	No commonly misidentified cell lines were used in this study.

Plants

Seed stocks	n/a
Novel plant genotypes	na/
Authentication	n/a